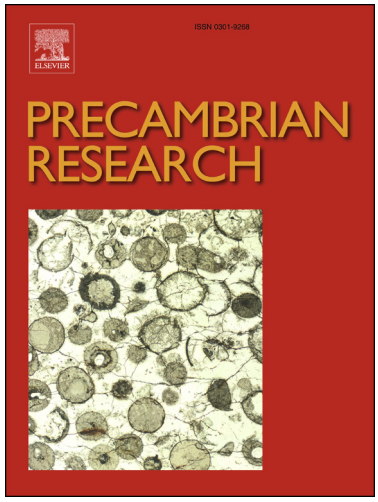

Depth-dependent δ ^{13}C trends in platform and slope settings of the Campbell-rand-Malmani carbonate platform and possible implications for Early Earth oxygenation

Suemeyya Eroglu, Mark van Zuilen, Heinrich Taubald, Kerstin Drost, Martin Wille, Elizabeth D. Swanner, Nicolas J. Beukes, Ronny Schoenberg

PII: S0301-9268(17)30101-8
DOI: http://dx.doi.org/10.1016/j.precamres.2017.09.018
Reference: PRECAM 4890

To appear in: *Precambrian Research*

Received Date: 27 February 2017
Revised Date: 15 September 2017
Accepted Date: 18 September 2017

Please cite this article as: S. Eroglu, M. van Zuilen, H. Taubald, K. Drost, M. Wille, E.D. Swanner, N.J. Beukes, R. Schoenberg, Depth-dependent δ ^{13}C trends in platform and slope settings of the Campbellrand-Malmani carbonate platform and possible implications for Early Earth oxygenation, *Precambrian Research* (2017), doi: http://dx.doi.org/10.1016/j.precamres.2017.09.018

Depth-dependent $\delta^{13}C$ trends in platform and slope settings of the Campbellrand-Malmani carbonate platform and possible implications for Early Earth oxygenation

Suemeyya Eroglu[1]*, Mark van Zuilen[2], Heinrich Taubald[1], Kerstin Drost[1,], Martin Wille[1], Elizabeth D. Swanner[3], Nicolas J. Beukes[4], and Ronny Schoenberg[1]

[1]Department of Geosciences, University of Tuebingen, Wilhelmstraße 56, 72074 Tübingen, Germany

[2]Institut de Physique du Globe de Paris, 1 rue Jussieu, 75238 Paris, France

[3]Department of Geological and Atmospheric Sciences, Iowa State University, 2237 Osborn Dr., Ames, IA 50011-1027, United States of America

[4]CIMERA, Department of Geology, University of Johannesburg, Auckland Park Kingsway Campus, 2006, South Africa

*Corresponding author: seroglu@geomar.de; present address: GEOMAR Helmholtz Centre for Ocean Research, Wischhofstraße 1-3, 24148 Kiel, Germany

Abstract

The evolution of oxygenic photosynthesis is widely seen as the major biological factor for the profound shift from reducing to slightly oxidizing conditions in Earth's atmosphere during the Archean-Proterozoic transition period. The delay from the first biogenic production of oxygen and the permanent oxidation of Earth's atmosphere during the early Paleoproteorozoic Great Oxidation Event (GOE) indicates that significant environmental modifications were necessary for an effective accumulation of metabolically produced oxygen. Here we report a distinct temporal shift to heavier carbon isotope signatures in lagoonal and intertidal carbonates ($\delta^{13}C_{carb}$ from -1.6 to +0.2 ‰, relative to VPDB) and organic matter ($\delta^{13}C_{org}$ from about -40 to -25 ‰, relative to VPDB) from the 2.58-2.50 Gy old shallow-marine Campbellrand-Malmani carbonate platform (South Africa). This indicates an increase in the burial rate of organic matter caused by enhanced primary production as well as a change from an anaerobic to an aerobic ecosystem. Trace element data indicate limited influx of reducing species from deep open ocean water into the platform and an increased supply of nutrients from the continent, both supporting primary production and an increasing oxidation state of the

platform interior. These restricted conditions allowed that the dissolved inorganic carbon (DIC) pool in the platform interior developed differently than the open ocean. This is supported by coeval carbonates from the marginal slope setting, which had a higher interaction with open ocean water and do not record a comparable shift in $\delta^{13}C_{carb}$ throughout the sequence. We propose that the emergence of stable shallow-water carbonate platforms in the Neoarchean provided ideal conditions for the evolution of early aerobic ecosystems, which finally led to the full oxidation of Earth's atmosphere during the GOE.

Keywords: Neoarchean carbonate platform; oxygen oasis; carbon isotopes; rare earth elements; carbonate diagenesis

1. INTRODUCTION

The record of the rise of free oxygen in Earth's atmosphere stimulates vigorous scientific debate, particularly as more sensitive geochemical proxies for oxygen have emerged during recent years. Even though the Great Oxidation Event (GOE) between about 2.42 to 2.33 Gy ago (Bekker et al., 2004; Farquhar et al., 2000; Gumsley et al., 2017; Hannah et al., 2004; Luo et al., 2016; Pavlov and Kasting, 2002) marks the first significant global rise of atmospheric oxygen above 10^{-5} of the present atmospheric level (PAL) (Farquhar et al., 2000), there are several indications for global (Crowe et al., 2013; Frei et al., 2009) or at least local accumulation of free oxygen hundreds of millions of years earlier, causing oxidative cycling of redox-sensitive elements (Anbar et al., 2007; Duan et al., 2008; Eroglu et al., 2015; Kendall et al., 2010; Kurzweil et al., 2015; Planavsky et al., 2014; Wille et al., 2007). In a largely anoxic world, it was necessary to increase the oxygen production and to decrease the oxygen consumption by reducing species to ultimately gain a net production of oxygen. It has been suggested that the formation of large, stable cratons during Meso- to Neoarchean times allowed the development of shallow-marine shelves, upon which large-scale stromatolitic carbonate platforms could grow, probably for the first time in Earth's history (Grotzinger, 1989; Hoffman, 1988; Hoffman and Grotzinger, 1988; Sumner and Grotzinger, 1996). The formation of such carbonate platforms could have increased primary production of organic matter. The transport of some organic matter

towards deeper settings and burial along the redox-stratified continental margin settings would consequently have sequestered it from respiration with oxygen or oxygen-derived oxidants (Falkowski and Isozaki, 2008; Kump and Barley, 2007).

Some of these shelves' marine sediments exhibit geochemical and sedimentological features for transient oxygen in surface ocean water masses. The Neoarchean shallow marine Campbellrand-Malmani carbonate platform (CMCP, Transvaal Supergroup, South Africa), for example, has (i) high abundances of authigenic rhenium and molybdenum in shales indicating redox-cycling of these elements fostered by oxidative weathering combined with reductive adsorption in these marine sediments (Wille et al., 2007); (ii) heavy molybdenum isotope signatures in black shales (Eroglu et al., 2015; Wille et al., 2007) and microbial carbonates (Eroglu et al., 2015; Voegelin et al., 2010) that indicate the presence of oxidized molybdenum in the form of molybdate in the water column, (iii) heavy nitrogen signatures in slope dolostones and mudrocks that might reflect the onset of oxic nitrogen cycling (Godfrey and Falkowski, 2009). Similar observations are reported for marine sediments from the Hamersley basin (2.6 Ga, Australia), showing heavy Mo isotope signatures (Duan et al., 2010) and authigenic enrichment of redox-sensitive elements (Anbar et al., 2007) in mudrocks, and C isotope signatures of organic material that imply a shift from an anaerobic to an aerobic ecosystem (Eigenbrode and Freeman, 2006; Eigenbrode et al., 2008). The carbonate platform of Steep Rock (2.8 Ga, Canada) also provides organic C isotope signatures (Grassineau et al., 2006) that were interpreted as signs of oxygen photosynthesizers, which is reinforced by the appearance of a mild negative Ce anomaly in the very shallow water carbonates (Riding et al., 2014) and argues for a stratified water column with oxygenated shallow water and anoxic deeper water. Biomarkers from the slope succession of the CMCP were interpreted as indicator of an aerobic ecosystem (Brocks et al., 1999; Waldbauer et al., 2009), however, more recent studies found that those samples suffered from contamination and question the suitability of Archean rocks for biomarker studies (Brocks, 2011; French et al., 2015).

The similarities of those geochemical 'fingerprints' suggest that Archean carbonate platform settings represent 'oxygen oases' (Olson et al., 2013; Riding et al., 2014). Fischer (1965) first used this expression to describe a restricted pool of net oxygen production, which might have reached oxygen

levels of up to 0.08 PAL (Kasting, 1991, 1992), in an otherwise anoxic world. The production and the accumulation of oxygen within platform 'oases' would have occurred effectively due to limited influx of upwelling deep ocean water masses (Sumner and Beukes, 2006), which contain chemically reducing hydrothermal species. Before the evolution of oxygenic photosynthesis, the reducing Archean environment was presumably dominated by an anaerobic microbial biosphere, probably largely based on chemolithoautotrophic microorganisms centered near hydrothermal vents (Nisbet and Sleep, 2001). Early forms of anoxygenic photosynthesis depended on reduced hydrothermal fluids, using dissolved H_2, H_2S or Fe(II) as electron donors for their metabolism. This situation drastically changed with the evolution of oxygenic photosynthesis (Des Marais, 2001). This form of metabolism marked a major innovative step in the evolution of life, since it allowed microorganisms to use water itself as a source of electrons and therefore enabled photosynthetic organisms to diversify into the photic zone of any aquatic setting, sovereign from hydrothermal flux. The release of free molecular oxygen subsequently triggered the shift towards an aerobic biosphere, dominated by oxygenic photosynthesis and heterotrophic respiration (Eigenbrode and Freeman, 2006; Kasting and Siefert, 2002). The model of Olson et al. (2013) confirmed that a decreasing availability of other hydrothermal electron donors (e.g. Fe(II) and H_2S) diminished the dominance of anoxygenic and oxygenic phototrophs and therefore the spatial extend of oxygen oases and oxygen concentrations maybe up to 10 µM (Reinhard et al., 2013). Riding et al. (2014) proposed a minimum oxygen concentration in Archean shallow seawater of 10.25 µM based on siderite-calcite equilibrium calculations, which corresponds an oxygen level of 0.06 PAL and is therefore similar to the value of 0.08 PAL suggested previously by Kasting (1991, 1992). However, even though oxygen might have been produced on those sites, it was probably not sufficient to globally oxidize the atmosphere. Any oxygen released from the ocean water would have been immediately consumed by the reducing atmosphere (Olson et al., 2013). Alternatively, the existence of terrestrial microbial mats could have allowed local oxidation on land and thus not necessarily within the shallow marine environment (Lalonde and Konhauser, 2015; Reinhard et al., 2013). An 'oxygen oasis' analogue in the Antarctic shows that microbial mats can contain high amounts of oxygen without even temporarily oxidizing the overlying anoxic water

column (Sumner et al., 2015), a scenario that has also been postulated for the Precambrian world by Herman and Kump (2005).

A drastic change in the ecosystem of carbonate platforms implies modifications in the carbon cycle along continental margins during the Late Archean, considering the importance of organic carbon as oxygen sink. Consequently, reported changes in the carbon isotope signature of organic carbon due to a shift from anaerobic to aerobic ecosystems imply a similar change in carbon isotope signatures of coeval carbonate carbon. In this study, we present new $\delta^{13}C_{carb}$, $\delta^{13}C_{org}$, $\delta^{18}O_{carb}$, trace element, and Raman data from carbonate and mudrock samples of two drill cores (KMF-5 and BH-1) from the lagoonal and peritidal facies of the CMCP. The combination of our data with previously published data from BH-1, GKP01 and GKF01 drill cores (Fischer et al., 2009), the latter two representing the platform margin/slope facies, allows the first investigation of environmental requirements for oxygen accumulation and reconstruction of the carbon cycle of a complete shallow-water platform, from deep subtidal to supratidal settings. Results show a mild shift towards heavier $\delta^{13}C_{carb}$ in the peritidal shelf environment towards the top of the stratigraphic succession. Typically, diagenetic overprint leads to a shift towards lighter $\delta^{13}C_{carb}$ signatures due to diagenetically altered organic matter (e.g. Derry, 2010a; Derry, 2010b; Jiang et al., 2012). Based on geochemical and spectroscopic data, we can exclude that this shift is caused by diagenetic overprint. Instead, a shift towards heavier $\delta^{13}C_{carb}$ signatures indicates the development of an isotopically heavier dissolved inorganic carbon (DIC) pool in the shallow ocean, probably because of organic carbon flux along a redox stratified water column.

2. GEOLOGICAL OVERVIEW

The CMCP represents the lower Transvaal Supergroup and was deposited between ~2.58 and 2.50 Ga (Sumner and Beukes, 2006) on the Kaapvaal Craton in southern Africa (Fig. 1 a). The platform facies of the CMCP is up to 2400 m thick (Fig. 1 b) and is preserved in the Malmani Subgroup in the Transvaal area (TA) and the Campbellrand Subgroup in the Griqualand West area (GWA). The Malmani Subgroup mainly consists of peritidal dolomitic stromatolites, which show varying degrees of silicification and are interbedded with siliciclastic mudrock layers. The Campbellrand Subgroup shows stromatolitic structures reflecting shallow subtidal depositional conditions. The slope facies is

preserved in the Campbellrand Subgroup of the GWA and the Prieska area and has a much lower thickness of up to 1000 m, whereby the basinal facies is even thinner (~500 m). The depositional conditions of the CMCP have been reconstructed in geochemical and sedimentological studies of four drill cores, the GKP01 and GKF01 drill cores from the Prieska facies, the BH-1 drill core from the GWA, and the KMF-5 drill core from the TA (Beukes, 1987; Eroglu et al., 2015; Knoll and Beukes, 2009; Schröder et al., 2006; Sumner and Beukes, 2006). Here, the focus is on the platform shelf, represented in the sediments of the KMF-5 and the BH-1 drill cores, as well as the Kuruman Kop outcrop, which contains carbonates from the shelf facies of the upper Campbellrand Subgroup (Beukes and Gutzmer, 2008; Kamber and Webb, 2001; Sumner, 2002). Well-preserved dolomite intervals were sampled for this study, with good preservation of sedimentary textures and structures. Veined, crackle brecciated, and coarsely recrystallized intervals were avoided. Additionally, samples of silicified dolomite and siliciclastic mudrocks were taken. Detailed descriptions of KMF-5 and BH-1 are provided by Eroglu et al. (2015) and Altermann and Siegfried (1997), respectively. Except for some carbonate segments in the eastern TA that were affected by high-temperature contact metamorphism related to the intrusion of the Bushveld Complex (Frauenstein et al., 2009), the majority of the CMCP experienced conditions no higher than lower greenschist facies metamorphism (Button, 1973; Miyano and Beukes, 1984).

Following the sedimentological studies by Beukes (1987) and Sumner and Beukes (2006), this study divides the CMCP into a lower and an upper section. The *lower CMCP*, mostly reflects a steep ramp architecture and includes the stratigraphical correlative formations Lower Nauga from the Campbellrand Subgroup (GKP01, GKF01; Prieska Area), Reivilo and the Kamden Member from the Campbellrand Subgroup (BH-1; GWA), and Oaktree and Monte Christo from the Malmani Subgroup (KMF-5; TA). The *upper CMCP* reflects the rimmed margin architecture and includes the formations of Upper Nauga from the Campbellrand Subgroup (GKP01, GKF01; Prieska Area), Fairfield, Klipfonteinheuwel, Papkuil, Klippan, Kogelbeen, and Gamohaan from the Campbellrand Subgroup (BH-1; GWA), and Lyttleton and Eccles from the Malmani Subgroup (KMF-5; TA). Sedimentology of the succession reveals that the CMCP experienced several trans- and regression events during changing influx of water masses from the open ocean and from the continent. The Kamden Member, a

1 to 2 m thick Fe formation layer preserved in the Prieska area and the GWA, was deposited between the lower and the upper CMCP. The TA does not contain the Kamden Member. However, a Fe-rich (10.34 wt-% Fe2O3) and silicate rich carbonate layer (sample 1265.1) in the upper Monte Christo Formation of the Malmani Subgroup could be stratigraphically correlative (Eroglu et al., 2015).

3. ANALYTICAL METHODS

3.1. ICP-MS analyses

Approximately 50 mg of sample powder were dissolved in ca. 5 g 2 % HNO_3 overnight at room temperature. Dissolved samples were centrifuged for 10 minutes at 5000 rpm. Subsequently, ca. 0.5 g of the supernatant was diluted with ca. 15 g of 1 ppb In and Re solution in 2% HNO_3 (internal standard). Trace element analyses were performed using an ESI SC-2DX autosampler coupled to a Thermo Fisher Scientific iCAP Qc® quadrupole ICP-MS instrument (Isotope Geochemistry Group, University of Tuebingen). Concentration data of the samples were derived from normalization of the oxide corrected ion signals to those of W2 international rock standard (U.S. Geological Survey) and from internal standardization to correct for instrumental drift and differences in ionization efficiency. Within-session accuracy was monitored by repeated analyses of international rock standards BHVO-2 and SCo-1 (U.S. Geological Survey). Depending on the element, deviations from the reference values (Marx and Kamber, 2010) were ≤1.8% for the well characterized BHVO-2 reference material and <5% for SCo-1.

3.2. Total organic carbon (TOC)

Total organic carbon (TOC) and total carbon (TC) contents were determined on mudrock samples, as well as silicified, and unsilicified carbonates. Approximately 0.8 g of sample powders was decalcified in 15 ml centrifuge tubes by drop-wise addition of 16 % HCl to remove all inorganic carbon (TIC). Residual samples were centrifuged for 10 min at 2000 rpm, decanted and again mixed with approximately 10 mL Milli-Q water. This procedure was repeated 7 to 10 times until samples were neutralized. Upon complete drying of the samples, between 5 to 70 mg, depending on the estimated TOC content, of decalcified samples (for TOC analyses) and un-decalcified samples (for TC analyses)

were weighed into tin-capsules. TOC and TC measurements were done with a VARIO EL Elemental Analyzer (ZAG, University of Tuebingen) and with an Elemental Analyzer NC2500 (Isotope Geochemistry Group, University of Tuebingen) by combustion at 950°C.

3.3. Carbon and oxygen isotope analyses

Analyses of $\delta^{13}C_{carb}$ and $\delta^{18}O_{carb}$ were performed using a Finnigan MAT 252 gas source mass spectrometer combined with a Thermo-Finnigan Gasbench II/CTC Combi-Pal autosampler (Isotope Geochemistry Lab, University of Tuebingen). Both devices are connected using the continuous flow technique with a He stream as carrier gas. This setup allows for online preparation of carbonate samples. About 0.1 mg dried sample powder is loaded into a 10 ml glass vial, sealed with a rubber septum. The vials are placed in an aluminum tray and set to 90°C. After purging with pure He gas, 20 drops of 99% phosphoric acid are added. After a minimum reaction time of 2.5 hours, released CO_2 is transferred (using a GC gas column to separate other components) to the mass spectrometer using a He carrier gas. The sample CO_2 is measured relative to an internal laboratory tank gas standard which is calibrated against in house (Laaser marble) and international (NBS18, NBS19) carbonate standards. All values are given in ‰ relative to Vienna PeeDee belemnite standard (VPDB) for $\delta^{13}C$ (Craig, 1957) and VPDB for $\delta^{18}O$ (Craig, 1957). The external reproducibility is ± 0.1‰.

Analyses of $\delta^{13}C_{org}$ were conducted on an Elemental Analyzer NC2500 connected to a Thermo Quest Delta Plus XL mass spectrometer in continuous flow online-mode. Decalcified samples (see TOC analyses for further details) containing 0.05 mg carbon were weighed in tin capsules and combusted at 1050°C in an oxidation tube and at 650°C in a reduction tube, before they were cooled in a watertrap and transferred through a GC gas column into the mass spectrometer. Sample C was measured relative to an internal acetanilide standard which is calibrated against in house (e.g. Laaser marble) and international (USGS24) standards.

3.4. Raman analyses

Raman analyses were performed at the Institute de Physique du Globe de Paris. Selected carbonate and mudrock samples from KMF-5 and Kuruman Kop are prepared as thin sections with 30 µm

thickness and polished down to 1 µm. Raman measurements were conducted on a Renishaw InVia Raman Microscope coupled to an Olympus BX61 confocal microscope, using an Ar monochromatic 514 nm laser source. Laser excitation was adjusted to an on-sample intensity of 0.4 mW at 2 x 20 s exposure time. Sample spots were focused with a 50x objective at 2 to 3 µm spots and acquisition was obtained in static mode within a range from 100 to 2000 cm^{-1}, centered at 1150 cm^{-1}. Beam centering and Raman spectra calibration were performed on a Si chip with a Raman band at 520.4 cm^{-1}.

4. RESULTS

4.1. Rare Earth Element and Yttrium (REE+Y) spectra

Typical REE+Y features of Archean seawater are depleted in light REE and have positive La anomalies, as well as Y/Ho ratios higher than 27, which is the value of post-Archean Australian Shale (PAAS) (Bau, 1999; Bau and Dulski, 1999; Kamber and Webb, 2001; Webb and Kamber, 2000). In carbonates, these indicators are strongly influenced by mixing water masses from the continent and from hydrothermal vents (Allwood et al., 2010; Kamber and Webb, 2001). Freshwater carries a continental signature (e.g. 'PAAS') and would thus even the seawater REE+Y pattern in affected carbonates (Kamber and Webb, 2001 and references therein). A higher input of hydrothermal waters is typically reflected by more pronounced positive Eu anomalies and decreasing Y/Ho ratios (Allwood et al., 2010; Derry and Jacobsen, 1990). In seawater with sufficient oxygen levels, Ce^{3+} is oxidized to Ce^{4+} and subsequently removed from the water column by adsorption on minerals surfaces. This results in a negative Ce anomaly, which can be reflected in the carbonates precipitated from that seawater (Webb and Kamber, 2000). However, Ce oxidation and therefore the development of a negative Ce anomaly is inhibited when Fe and Mn concentrations in the seawater are higher than 50 nM (Seto and Akagi, 2008), as they lower the Eh. Thus, even Fe (and Mn) concentrations of a few µM in the shallow-marine environment, could inhibit the development of a Ce anomaly even during oxygen production.

Pure carbonates of KMF-5 and BH-1 were analyzed for their REE+Y distributions. Additionally, four mudrock samples and the Fe- and silicate-rich sample 1265.1 from KMF-5 were measured (concentrations are listed in Tables S1 and S2 in the supplementary material). Y/Ho anomalies were

calculated from absolute values. Concentrations were PAAS-normalized (index N) (Taylor and MacLennan, 1985) and La, Ce, and Eu anomalies were calculated. Positive La anomalies are indicated by La/La* values bigger than unity ($La/La^* = La_N/(Pr_N*(Pr_N/Nd_N)^2)$), negative Ce anomalies by Ce/Ce* values bigger than unity ($Ce/Ce^* = Ce_N/(Pr_N*(Pr_N/Nd_N)^2)$), and positive Eu anomalies by Eu/Eu* values bigger than unity ($Eu/Eu^* = Eu_N/(Sm_N*(Sm_N/Nd_N)^2)$) (Lawrence and Kamber, 2006; Webb and Kamber, 2000).

From KMF-5 almost all carbonate samples reveal positive La (mean 1.268 ± 0.508 (2σ)) and Eu (mean 1.332 ± 0.448 (2σ)) anomalies as well as Y/Ho ratios higher than PAAS (mean 40 ± 26 (2σ)). None of them shows any significant Ce anomaly (mean 1.084 ± 0.156 (2σ)). Mudrock samples show La/La* and Ce/Ce* values of 1.094 to 1.540 and 0.953 to 1.394 , respectively, and have Y/Ho ratios between 23 to 28. Eu/Eu* is mostly below or around unity (0.613 to 1.046) and only shows a clear positive anomaly in sample 1265.1 (1.197). Carbonates of BH-1 reveal more pronounced Y/Ho ratios (mean 72 ± 31) and La anomalies (mean 1.402 ± 0.464). Eu anomalies are detectable (mean 1.291 ± 0.314) but no Ce anomalies (1.048 ± 0.079).

4.2. Total organic carbon (TOC)

TOC values of KMF-5 pure carbonates (Table S3, supplementary material) lie between 0.01 and 0.17 wt-% (mean with 2σ: 0.03 ± 0.07 wt-%). TOC of silicified carbonates range from 0.01 to 0.15 wt-% (0.06 ± 0.09 wt-%). TOC values for detritus-rich carbonates are significantly higher, between 0.14 and 3.57 wt-% (1.80 ± 2.52 wt-%). TOC values in mudrock samples obtain a wide range between 0.83 and 8.50 wt-% (2.90 ± 4.14 wt-%). Pure carbonate samples of the BH-1 show TOC values between 0.01 and 0.29 wt-% (0.07 ± 0.13 wt-%) and two detritus-containing carbonates 340 and 375 show higher values of 0.28 and 0.20 wt-%, respectively (Table S4, supplementary material).

4.3. Carbon and oxygen isotopes

Pure carbonates of KMF-5 (Table S3 and Fig. S1, supplementary material) show a range in $\delta^{18}O_{carb}$ signatures between -10.0 and -6.2 ‰ (mean with 2σ: -8.0 ± 1.5 ‰). Silicified carbonates range from -10.3 to -5.4 ‰ (-7.6 ± 2.1 ‰), detritus-containing carbonates from -12.0 to -7.5 ‰ (-8.7 ± 2.8

‰), and mudrocks from -17.1 to -8.0 ‰ (-13.9 ± 6.0 ‰). For $\delta^{13}C_{carb}$, pure carbonates range between -0.9 and +0.3 ‰ (-0.4 ± 0.6 ‰). Silicified carbonates show values between -1.2 and +0.4 ‰ (-0.2 ± 0.8 ‰). Detritus-containing carbonates range from -1.0 to +0.1 ‰ (-0.6 ± 0.7 ‰), and mudrocks from -12.3 to -0.6 ‰ (-5.3 ± 7.9 ‰). The Fe- and silicate-rich sample 1265.1 shows relatively low $\delta^{18}O_{carb}$ and $\delta^{13}C_{carb}$ values of -16.4 and -3.2 ‰, respectively. For $\delta^{13}C_{org}$, pure carbonates range between -28.5 and -21.6 ‰ (-25.4 ± 3.5 ‰), silicified carbonates from -28.6 to -20.5 ‰ (-25.2 ± 4.7 ‰), detritus-containing carbonates from -33.2 to -22.2 ‰ (-29.5 ± 6.2 ‰), and mudrocks from -39.4 to -21.8 ‰ (-32.0 ± 8.5 ‰).

Pure carbonates of BH-1 rocks (Table S4 and Fig. S2, supplementary material) yield $\delta^{18}O_{carb}$ values between -13.2 and -7.7 ‰ (mean with 2σ: -9.5 ± 2.8 ‰), $\delta^{13}C_{carb}$ signatures between -1.1 and -0.1 ‰ (-0.6 ± 0.6 ‰), and $\delta^{13}C_{org}$ signatures between -33.4 and -23.3 ‰ (-29.8 ± 4.5 ‰). Fe-rich carbonate 1914 shows values of -7.7 ‰ ($\delta^{18}O_{carb}$), -1.3 ‰ ($\delta^{13}C_{carb}$), and -28.9 ‰ ($\delta^{13}C_{org}$). Detritus-rich carbonates 340 and 375 show values of -11.5 ‰ and -9.6 ‰ ($\delta^{18}O_{carb}$), -0.1 ‰ and 0.1 ‰ ($\delta^{13}C_{carb}$), and -35.1 ‰ and -33.4 ‰ ($\delta^{13}C_{org}$), respectively.

4.4. Raman spectra of organic matter

Raman spectroscopy detects the structural order of carbonaceous material (CM), which is best parameterized by the relative intensities of the so-called D ("disordered") and G ("graphite") bands, as well as their central peak positions and peak widths. The intensity ratio of the D- and G-bands (I_D/I_G) and width of the D-peak (FWHM-D) can be used to describe the degree of carbonization of organic material (Beyssac et al., 2002; Foucher et al., 2015; Lahfid et al., 2010; Olcott-Marshall et al., 2012; Sforna et al., 2014; Wopenka and Pasteris, 1993) (Fig. 2). With increasing degree of carbonization (a purely chemical process leading to a pure sp^2-carbon material, as defined by Rouzaud et al. (2015)) and graphitization caused by progressive diagenesis and low-grade metamorphism, the FWHM-D will become smaller (from > 200 cm^{-1} to ca. 50 cm^{-1}) and the I_D/I_G-ratio will increase (from ca. 0.8 to more than 2). Further alteration at higher temperatures will cause graphitization (a purely physical process of reorganization into triperiodic order, as defined by Rouzaud et al. (2015)). This process of graphitization causes the FWHM-D to further decrease (from ca 50 cm^{-1} to ca 35 cm^{-1}), while the I_D/I_G

ratio decreases steadily to 0 (at granulite facies metamorphism). In well-characterized terrestrial kerogen, D- and G-band characteristics allow to determine the peak metamorphic temperatures experienced by the material, because the structural changes due to heating are usually irreversible (Beyssac et al., 2004; Beyssac et al., 2002; Lahfid et al., 2010). The geothermometer of Beyssac et al. (2002) is calibrated over the temperature range of 330-650 °C, and the geothermometer of Lahfid et al. (2010) over the temperature range of 200-320 °C. Since the CMCP experienced lower greenschist facies metamorphism (Button, 1973; Miyano and Beukes, 1984), it is expected that the carbonaceous material in samples studied here will display Raman spectral characteristics that directly overlap the lower limit of the Beyssac et al. (2002) geothermometer and the upper limit of the Lahfid et al. (2010) geothermometer. It is therefore difficult to apply these thermometers and instead the approach described in Delarue et al. (2016) is used, in which simple Raman spectral indicators of a carbonaceous sample are compared to those of the known carbonization continuum of organic materials. In order to do so, our data are reported as the ratio of the peak intensities of the D- and G-bands (I_D/I_G) and the width of the D band (FWHM-D) (following the protocol described in Sforna et al. (2014)).

Organic material of KMF-5 carbonates and mudrocks yield I_D/I_G ratios between 1.2 and 2.1 and FWHM-D values between 39 and 71 (Table S5, supplementary material). Mudrock samples 665.1 and 665.3 show the lowest FWHM-D values and have been apparently exposed to higher metamorphic conditions than the rest of the analyzed samples (Fig. 2). Those two samples excluded, the remaining KMF-5 samples obtain FWHM-D values between 44 and 71.

Carbonate samples from Kuruman Kop reveal more ‘disordered’ signatures for organic material than those of KMF-5, with I_D/I_G ratios between 0.7 and 0.9 and FWHM-D values between 78 and 103 (Table S5, supplementary material).

5. DISCUSSION

5.1. Diagenetic overprint of the CMCP shelf succession

The geochemical and isotopic composition of marine carbonates can reflect the primary conditions during their precipitation. However, in reality these primary signatures are often secondarily altered by hydrothermal fluids and/or freshwater. The Transvaal Area was intruded by the 2.054 Ga old Bushveld igneous complex (Buick et al., 2001) (Fig. 1a) and contact-metamorphic overprint of adjacent carbonates has been described by Frauenstein et al. (2009). Moreover, early diagenetic dolomitization and silicification affected large parts of the CMCP and signal interaction of seawater with freshwater (Beukes, 1987; Eroglu et al., 2015). Thus, different geochemical proxies were examined carefully to unravel primary and potential secondary signals and to avoid misinterpretation. Potential effects of secondary fluid alteration during diagenesis and contact metamorphism were tested here by $\delta^{18}O_{carb}$ and elemental composition. Careful determination of peak metamorphic conditions and post-depositional overprint of the samples was crucial in order to evaluate the potential of preservation of the original geochemical signatures and were investigated by Raman spectroscopy. In the following the preservation of geochemical signatures will be carefully evaluated and subsequently the paleoenvironmental conditions of the CMCP will be reconstructed based on those findings.

5.1.1. Evaluation of the influence of the Bushveld intrusion on the Malmani Subgroup

The Bushveld magmatic complex intruded the carbonate platform in the Transvaal Area (Fig. 1a). Secondaryly grown minerals such as garnet, pyroxene, siderite, and ankerite are abundant in the carbonates near the contact aureole (Frauenstein et al., 2009) and point to strong recrystallization and alteration due to high-T fluid circulation. Although the rocks of KMF-5 are in c. 80 km distance and thus not in direct contact with the main Bushveld intrusion, they are intersected by a few mafic dykes (Eroglu et al., 2015). The latter are probably related to the emplacement of the Bushveld complex and caused alteration of the adjacent carbonate sections resulting in the formation of secondary siderite and ankerite. Apart from these spatially limited alteration zones, which were avoided during sampling, the carbonate rocks in the drill core show no macroscopic signs of secondary mineral growth induced by the Bushveld complex. Carbonates of the far more distant Griqualand and Prieska area (Campbellrand Subgroup; BH-1, GKP01, GKF01; Fig. 1b), are unaffected by the Bushveld complex (Beukes, 1987).

Based on $\delta^{18}O_{carb}$ analyses, Frauenstein et al. (2009) observed that the degree of fluid alteration in the sedimentary country rocks of the Transvaal area decreases with increasing distance from the Bushveld complex. Three kilometers from the contact zone, $\delta^{18}O_{carb}$ values are as low as -22 ‰ and interpreted to be the result of intense fluid-rock interaction. With increasing distance, $\delta^{18}O_{carb}$ values increase continuously to ~ -10 ‰ at 18 km distance from the contact. Such high isotope values probably reflect rather pristine, marine signatures (Crne et al., 2014) and are close to the best estimate for Neoarchean seawater ($\delta^{18}O_{carb}$ ~ -8 ‰) (Fig. 3 a and b) (Shields and Veizer, 2002; Veizer et al., 1999). Pure and silicified carbonate rocks of KMF-5 (Table S3 and Fig. S1 in supplementary material) yield $\delta^{18}O_{carb}$ values between -10.3 to -5.4 ‰ (mean with 2σ: -7.8 ± 1.8 ‰), similar to stratigraphically correlative carbonate sequences of the GKP01 (-8.2 ± 3.9), GKF01 (-7.6 ± 1.8 ‰) (Fischer et al., 2009), and BH-1 (-9.5 ± 2.8 ‰), which are unaffected by the Bushveld magmatic fluids. The $\delta^{18}O_{carb}$ values of GKP01 and GKF01 were obtained from micritic microbialites (Fig. 4) (Fischer et al., 2009; Horstmann and Beukes, 2002). In contrast, some other samples from all four drill cores are coarse-grained, show secondary carbonate veins, and yield significantly lighter $\delta^{18}O_{carb}$ values (down to -17 ‰), possibly due to alteration by fluids produced during devolatilization reactions or intense recrystallization (Figs. 3, 4) (Fischer et al., 2009; Horstmann and Beukes, 2002; Valley, 1986). Thus, $\delta^{18}O_{carb}$ values of here analyzed KMF-5 carbonates do not show any indication for diagenetic overprint by magmatic fluids. In an earlier study by Eroglu et al. (2015) the pristine nature of some other geochemical signatures of these carbonates has been suggested, in particular that of the Fe and Mn concentrations (see section 5.1.4.), which are controlled by the depositional depth below sea level as well as different solubility behavior (Beukes, 1987; Beukes and Gutzmer, 2008). As the exposure to magmatic fluids from the Bushveld complex would have led to an obliteration of the water depth related signal, an impact of such fluids on the majority of the rocks can be ruled out. Furthermore, the interaction of the carbonates with magmatic fluids is expected to produce very positive Eu anomalies, no Y anomaly as well as an overall slight increase in the abundance from light REE to heavy REE (relative to PAAS) (Maier and Barnes, 1998). None of the REE+Y spectra obtained in our study show such signatures. In summary, visual inspection, geochemical features, and oxygen isotope signatures

of the studied samples do not reveal any indication of secondary fluid alteration resulting from the emplacement of the Bushveld igneous complex.

5.1.2. Preservation of organic material and metamorphic conditions

The CMCP has been described as one of the best preserved Archean platforms, which was metamorphosed very early under lower greenschist facies conditions (Button, 1973; Miyano and Beukes, 1984). However, amphibolite facies metamorphism has been observed near the contact to the Bushveld complex (Frauenstein et al., 2009). Thus, Raman analyses were conducted to examine the degree of alteration of organic matter in KMF-5 samples from the TA and Kuruman Kop samples from the GWA and to evaluate the quality of $\delta^{13}C_{org}$ signatures. Organic material throughout KMF-5 displays a continuum from an I_D/I_G ratio of 1.3 and a FWHM-D of 70 to an I_D/I_G ratio of 2.1 and FWHM-D of 45, which overlaps with the carbonization continuum presented by Delarue et al. (2016) and confirms regional lower greenschist-facies metamorphism in the TA (Table S5 in supplementary material; Fig. 2). These samples show a large spread in $\delta^{13}C_{org}$ from -39.4 to -24.0 ‰. It should be noted, however, that the $\delta^{13}C$ signature of organic material can be shifted toward heavier values already under greenschist facies conditions (Valley and O'Neil, 1981). Two mudrock samples, 665.3 and 673.0 (KMF-5), are more altered and show signs of early graphitization (I_D/I_G = 1.2-1.5, FWHM-D = 39-47). Clearly, they experienced a higher peak metamorphic temperature, which is also indicated by heavy $\delta^{13}C_{org}$ signatures of -22.9 and -21.8 ‰, respectively. The strongly silicified character of these samples suggests that they were pervasively altered by fluids and are likely to have lost their primary $\delta^{13}C_{org}$ signature. However, some other strongly silicified carbonate samples obtain similar FWHM-D values and $\delta^{13}C_{org}$ values as un-silicified samples (Table S3 in supplementary material). Therefore, silicification is not the only explanation for the stronger alteration of some samples and another factor had to be involved in this process. Outcrop samples from fenestral carbonate of the Kuruman Kop contain organic material that has experienced a lesser degree of carbonization than that found in KMF-5, as indicated by a range of I_D/I_G = 0.73-0.93, FWHM-D = 78-103 (Fig. 2). Carbonates from the same formation in the BH-1 yield $\delta^{13}C_{org}$ values from -29.9 to -27.0‰ (Table S4 in supplementary material). Furthermore, only a slight discrepancy in $\delta^{13}C_{org}$ values between mudrocks

and carbonates in the slope region has been described (Fischer et al., 2009) in contrast to a larger offset between different lithologies in the peritidal region of the TA, as it is implied by mudrock sample 867.3 ($\delta^{13}C_{org}$ = -39.4 ‰) and the stratigraphically close carbonate sample 884.9 ($\delta^{13}C_{org}$ = -28.0 ‰) (KMF-5; Table S3 in supplementary material; Fig. 5). Although we acknowledge the possibility that some rock samples of KMF-5 were affected by higher temperatures, which might have caused an isotope shift in organic carbon toward slightly heavier values, there are more reliable indicators that primary signatures were indeed preserved. First, the majority of $\delta^{13}C_{org}$ data of Transvaal and Griqualand West samples overlap (Fig. 5), revealing that higher peak metamorphic temperatures for the Transvaal area play a minor role for a shift in isotope values. Second, the abovementioned samples 867.3 and 884.9 are two of the least affected samples of KMF-5 regarding their Raman spectral characteristics (I_D/I_G down to 1.39 and 1.27, FWHM-D up to 71 and 66, respectively), and therefore argue for the actual preservation of their primary signatures, which are dependent upon the depositional environment. Third, $\delta^{13}C_{org}$ signatures depend on the fractionation of carbon by different microbial species. As microbial mats contain communities of several microbial species, the $\delta^{13}C_{org}$ signatures therefore rather reflect mixed signals of these species, and that a trend to lighter or heavier signatures can give us information about the dominant microbial species, depending on available nutrients, electron donors, light and other environmental factors. Thus, we propose for KMF-5 samples with a high FWHM-D that a large isotope difference of $\delta^{13}C_{org}$ between carbonates and mudrocks is likely related to different microbial respiration pathways during different depositional conditions, i.e. a stronger influence of cyanobacteria in the very shallow marine microbial mats, alternating with more anaerobic microbial activity during the deposition of mudrocks.

5.1.3. Effect of early diagenesis on carbon and oxygen isotope signatures

Carbonate rocks of the Malmani Subgroup (TA) are fully dolomitized and partly silicified (Eroglu et al., 2015), similar to carbonates of the Campbellrand Subgroup (GWA), which are almost fully dolomitized except of some sections that remained calcitic (Beukes, 1987). Dolomitization is the replacement of calcite by dolomite, according to the equation proposed by Lippmann (1973) and Morrow (1982),

$(2-x)CaCO_3 + Mg^{2+} + xCO_3^{2-} \rightarrow CaMg(CO_3)_2 + (1-x)Ca^{2+}$ (x: mole)

and is usually initiated by large-scale fluid flow through soft sediments and interaction between calcium-carbonate and Mg-rich saline pore fluids from seawater, which is the main source of Mg^{2+} (Purser et al., 1994). Kinetic hindrance of dolomitization can be overcome by an increase of the Mg^{2+}/Ca^{2+} ratio in the solution via evaporation (Land, 1985), a decrease of the ionic strength by dilution of seawater with freshwater (Folk and Land, 1975), and an increase of alkalinity (CO_3^{2-} anions) by dissolution of limestone (Murray, 1960). The evaporation of seawater, the formation of highly Mg-rich brines, and the pumping of this slightly hypersaline marine waters through a carbonate succession is one the most common models (Simms, 1984). However, to explain large-scale dolomitization of carbonate platforms, pumping of vast volumes of dolomite-oversaturated seawater through a carbonate succession has been suggested as main process (Kohout, 1967; Simms, 1984). In combination, these scenarios could explain why some parts of the Campbellrand Subgroup in the GWA still contains some limestone, whereas the Malmani Subgroup is fully dolomitized. Carbonates deposited near the platform margin would still have had better exchange with open ocean water, in contrast to the interior platform, where poor water circulation and restricted influx of fresh open marine water allowed the formation of Mg-enriched brines and thus enhanced the complete dolomitization of the Malmani Subgroup (Beukes, 1987).

The silicification observed in the upper succession of the Malmani Subgroup is fairly typical for Precambrian carbonate platforms, partly because Si concentrations in the seawater were significantly higher than today (Knauth, 1979). The replacement of carbonate by silicic phases is an early diagenetic process, caused by the interaction between marine and meteoric pore fluids in the mixing zone of near-shore sediments, and is favoured by increasing porosity, increasing salinity, decreasing pH, and increasing f_{CO2} (Knauth, 1979; Maliva and Siever, 1988, 1989; van den Boorn, 2008). In particular an increase in partial pressures of CO_2 combined with lower fluid pH are of importance and can lead to undersaturation of carbonate and oversaturation of silica, resulting in calcite dissolution and silica precipitation, respectively. An early diagenetic origin for the silicification in the Malmani Subgroup, as opposed to a possible later hydrothermal overprint, is supported by heavy $\delta^{30}Si$ values from +0.53 to +2.35 ‰ of silicified carbonate samples from the Eccles and the Monte Christo

formations (Eroglu et al., 2015). Modern surface waters like rivers (average $\delta^{30}Si$ of +0.8 ‰) and shallow seawater (average $\delta^{30}Si$ of +1.1 ‰) typically show such isotopically heavy Si signatures (De la Rocha et al., 2000; Georg et al., 2007; Ziegler et al., 2005), whereas hydrothermal fluids show signatures between -0.3 and +0.3 ‰ (Chakrabarti et al., 2012 and references therein; van den Boorn, 2008). The reason for the strong increase of silicification in the Eccles Formation (Eroglu et al., 2015) might be related to the platform architecture. Sumner and Beukes (2006) reconstructed that during the second half of platform growth a rimmed margin developed that promoted the formation of an interior lagoon. We suggest that the rimmed margin limited the exchange of open ocean water with the lagoon, which ipso facto increased the influence of freshwater on the platform interior. Poor mixing of lagoonal water with seawater and degradation of organic matter would thus result in a simultaneous increase in f_{CO2} and decrease in pH (Knoll, 1985; Siever, 1962). The low TOC content in the Eccles formation (Eroglu et al., 2015) argues for such an increase in organic matter oxidation/degradation. In modern coastal carbonates, the influx of meteoric waters from the continent can cause a shift to lighter $\delta^{18}O_{carb}$ signatures, if those meteoric waters are isotopically depleted. The influx of meteoric waters can also supply organic material from the continent, in particular land plants, that can be oxidized in the shallow-marine environment and induce a shift to lighter $\delta^{13}C_{carb}$ values (Holmden et al., 1998; Oehlert and Swart, 2014). Those effects would become visible during rise and fall of seawater level (Immenhauser et al., 2003). Even though the platform clearly experienced several of these trans- and regression events (Eroglu et al., 2015; Sumner and Beukes, 2006), such a trend to negative values related to sea-level change is not observed for the here investigated microbial carbonates, neither for $\delta^{13}C_{carb}$ nor for $\delta^{18}O_{carb}$ signatures (Fig. 6). Regarding the $\delta^{13}C_{carb}$, one explanation could be the lack of land plants during the Neoarchean, which would have affected the $\delta^{13}C_{carb}$ signature in very shallow marine settings towards lighter values (Holmden et al., 1998; Immenhauser et al., 2003). Instead, we observe a shift to slightly heavier values in the upper CMCP shelf succession (Fig. 6), which is discussed further in paragraph 5.3. Variations of $\delta^{18}O_{carb}$ values of the here investigated carbonates are between about -11 to -5 ‰ that might indicate syndepositional interaction with fluids during early diagenetic processes (Allan and Matthews, 1982; Immenhauser et al., 2003), like dolomitization and silicification. Indeed, early diagenetic dolomite formed in slightly hypersaline tidal flats can be about 2

‰ enriched in ^{18}O (Burdett et al., 1990; Veizer et al., 1992). Yet, we want to point out that over Earth history $\delta^{18}O_{carb}$ values constantly increased (Kasting et al., 2006) and the best estimate for Neoarchean seawater is thus about -8 ‰ (Shields and Veizer, 2002; Veizer et al., 1999). Thus, although some fluid interaction might have influenced the samples investigated here, they are still very well preserved, with some excursions to lighter $\delta^{13}C_{carb}$ values (Fig. 3 a), which can be explained by more intense fluid interaction and degradation of organic matter, e.g. via dissimilatory iron reduction (DIR).

5.1.4. Early diagenesis and geochemical signatures

Sedimentological and geochemical observations reveal that the distinctions between individual sediments of the CMCP were governed by water depth, water circulation, detrital supply from the adjacent land area and diagenesis (Beukes, 1987; Eroglu et al., 2015; Sumner and Beukes, 2006). Certain mineralogical (dolomitization and silicification) and geochemical (Mg and Si) signatures clearly changed during diagenesis (Beukes, 1987; Eroglu et al., 2015). Some studies note that other characteristic trace element patterns in carbonates indicate severe diagenesis and alteration that could overprint primary signals because of leaching and dissolution of siliciclastics, sulphides, and oxyhydroxides, which would result e.g. in a decrease of Sr and Na and an increase in Mn and Fe (Banner, 1995; Brand and Veizer, 1980; Veizer, 1983). Therefore, pure carbonates with little to no detrital component are promising targets reflecting primary seawater signatures (Webb and Kamber, 2000). The input of trace elements into the carbonate structure is dependent on the concentration of trace elements in the porewater, the water-rock ratio and the effective distribution coefficient. Thus, since freshwater can carry a continental trace element signature (Kamber and Webb, 2001 and references therein), it is likely that an aqueous continental source might have influenced the peritidal carbonates. In Figure 7, data of selected pure carbonates are plotted in a scatter diagram of Sr/Ca vs. Mn (modified after Veizer et al., 1989). Samples show depletion of Sr and enrichment of Mn relative to limestone, which is considered as typical signatures of carbonates after early diagenesis (Veizer, 1983; Veizer et al., 1989). The ionic radii of Mg^{2+}, Fe^{2+} and Mn^{2+} are very similar and their distribution coefficients are higher than unity, such that they are preferentially incorporated into the carbonate structure during dolomitization (Reeder, 1983). Sr^{2+} on the other hand substitutes for Ca^{2+}

and is subsequently lost during dolomitization (Kretz, 1982). Analyzed carbonates show similar Sr/Ca ratios and cannot be clearly distinguished with that parameter. However, if sorted after Mn concentrations, the samples can be distinguished between their depositional environments, namely peritidal and shallow subtidal depths (Fig. 7). According to Veizer et al. (1989), peritidal carbonates plot into the 'dolomite' field and shallow subtidal carbonates plot into the 'siderite' field. However, the shallow subtidal pure carbonates analyzed here are clearly dolomite and not siderite, based on geochemistry (Eroglu et al., 2015) and mineralogy (Fig. S3). Therefore, the mineralogical difference in Mn concentration has another origin. Eroglu et al. (2015) described how the Fe/Mn ratio (expressed as Fe# = $Fe_{tot}/(Fe_{tot}+Mn_{tot})$) in carbonates correlate with water depth and detrital input. The dependence of Fe and Mn concentrations from water depth is a result of the lower redox potential of Fe compared to Mn. This promotes Fe precipitation from more reducing, deeper water beyond the shelf area and Mn precipitation at shallower, more oxidized waters of the platform (Beukes, 1987). As a result, the Fe/Mn ratios of pure carbonates from basinal Prieska facies (Fig. 8) reported in Voegelin et al. (2010) (Fe# mean with 2σ: 0.52 ± 0.15) are slightly higher than those of the Campbellrand shelf facies (Fe# 0.31 ± 0.11) and the subtidal carbonates of the Malmani inner shelf facies (Fe# 0.39 ± 0.06) (Eroglu et al., 2015). Pure carbonates of the subtidal lower Oaktree Formation and the intertidal Monte Christo and Eccles formations show higher Fe/Mn ratios (Fe# 0.56 ± 0.16), contradicting the concept of preferential Fe precipitation over that of Mn at lower oxygen fugacity. The lower Oaktree Formation reveals the highest Fe/Mn ratio for pure carbonates in KMF-5 (samples 1790.1 and 1800.1 with Fe# values of 0.68 and 0.59, respectively) and might indicate a higher influx of open ocean water. Intertidal carbonates on the other hand are frequently intercalated by Fe-rich mudrocks, in particular the Monte Christo Formation (Fig. 8). It is possible that early-diagenetic processes released Fe from these mudrocks to the carbonates (Veizer, 1983). Freshwater might also have had an influence, as silicified carbonates also reveal higher Fe/Mn ratios (Fe# 0.56 ± 0.16) (Eroglu et al., 2015). Since freshwater can carry a continental trace element signature (Kamber and Webb, 2001 and references therein), it is likely that an aqueous Fe source from the continent might have influenced the peritidal carbonates. Nevertheless, the dependence of the Fe/Mn ratio in shallow subtidal carbonates from the TA and GWA on the water depth indicates that those signatures were

produced during very early dolomitization (Beukes, 1987), maybe within the first 1-2 Ma after deposition, as described for the Bahamian carbonate platform (Mcneill and Kirschvink, 1993; Swart et al., 1987), when the carbonate lattice incorporated Mg (together with Fe and Mn) from the coeval seawater. Carbonates from peritidal settings, however, seem to have been perturbed by detrital input and mixing with freshwater.

PAAS-normalized REE+Y distributions of pure carbonates (Tables S1, S2 in supplementary material) reflect varying mixtures of shallow seawater (Y/Ho anomaly > 27, positive La anomaly, depleted light REE over heavy REE), deeper open ocean water with a hydrothermal signature (positive Eu anomaly, depleted light REE over heavy REE), and meteoric water from the continent (Y/Ho around 27, even patterns) (Kamber and Webb, 2001 and references therein). Carbonates of the lowermost Oaktree Formation (1790.1 and 1800.1) show elevated heavy REE patterns, probably due to an enhanced hydrothermal influence (Allwood et al., 2010) at the beginning of carbonate growth during the first massive flooding along the Kaapvaal Craton (Fig. 9) (Sumner and Beukes, 2006). Lagoonal carbonates from the upper Oaktree Formation (KMF-5) and Reivilo Formation (BH-1) carry REE+Y signatures typical for shallow seawater (Fig. 9). A more pronounced average Eu anomaly of 1.99 and a lower average Y/Ho ratio of 48 for slope carbonates compared to coeval lagoonal carbonates with values of 1.28 and 75, respectively, reveal a diminished influence of open ocean water, which means hydrothermal influx, from the slope towards the shallow-water platform. This can be confirmed by Fe and Mn distributions (Fig. 8) (Eroglu et al., 2015). A stronger influence from meteoric water with ongoing platform growth becomes obvious from even REE+Y signatures in the peritidal Monte Christo and Eccles carbonates and partly in the lagoonal Lyttleton carbonates (Fig. 9). Alternatively, it is possible that peritidal carbonates were influenced by the REE+Y composition of adjacent mudrocks during early diagenesis, the same process that also caused elevated Fe# signatures in those carbonates.

5.2. Paleoenvironmental reconstruction of the CMCP

Even though most of the CMCP is dolomitized, sedimentological features and structures are still well preserved (Beukes, 1987; Eroglu et al., 2015; Sumner, 2002; Sumner and Beukes, 2006; Sumner and Grotzinger, 1996). Furthermore, REE+Y patterns as well as Fe and Mn concentrations of these rocks

can be correlated with the stratigraphy, the water depth, and the input of hydrothermal or continental fluids (Eroglu et al., 2015; Voegelin et al., 2010). This allows the reconstruction of some environmental conditions and the evolution of this carbonate platform. The Oaktree and Monte Christo formations (lower CMCP) contain abundant mudrock layers while none are contained in Lyttleton and only few mudrock layers in Eccles (upper CMCP). Additionaly, the Eccles formation contains abundant chertlayers (Eroglu et al., 2015). These trends seem independent of water depth but at least partly related to the platform architecture (Fig. 9). It is possible based on the geochemistry to distinguish between sedimentary facies that interacted with the open ocean, i.e. the slope environment and the early stages of steep platform architecture, and facies that indicate more restricted conditions on the platform (e.g. peritidal settings) due to the transition to a rimmed margin architecture. Thereby, four major stages of platform evolution can be distinguished (Fig. 9). During the initial flooding of the Kaapvaal Craton and incipient carbonate deposition, the samples of the lower Oaktree Formation show elevated Fe, Mn (Eroglu et al., 2015), and REE concentrations as well as REE+Y signatures that are characteristic for hydrothermal fluids from mid-ocean ridges (Pearce, 1983), defined by depleted light REE relative to the heavy REE. This changed with the build-up of the platform and a decreasing influx of open ocean (hydrothermal) water, so that the carbonates of the upper Oaktree Formation show REE+Y signatures characteristic for Archean shallow seawater, enriched in heavy REE relative to light REE and with a positive La and Y anomaly (Fig. 9) (Kamber et al., 2004). After the build-up of the steep ramp platform and during a regression, the peritidal Monte Christo Formation and the lagoonal Reivilo Formation were deposited. During this stage more continental material was deposited and was preserved as organic-rich mudrocks, which show REE+Y signatures of continental material (PAAS). The carbonates of the Monte Christo Formation are more depleted in REE+Y compared to the mudrocks, but show a distinct and even ‘continental’ pattern, defined by slighter La and Y anomalies and without a depletion of light REE over heavy REE, compared to the ‘seawater’ pattern of Oaktree and Reivilo carbonates (Fig. 9). We interpret that the Monte Christo carbonates were more strongly influenced by continental fluids. The Kamden ‘Iron Formation’ Member was deposited during a temporary major transgression and is geochemically visible in Fe-rich rocks throughout the platform (Sumner and Beukes, 2006). The Fe- and detritus-rich sample 1265.1 in KMF-5 shows a

REE+Y pattern that resembles a mudrock composition and is close to PAAS. However, in contrast to the mudrocks, 1265.1 also reveals a positive Eu anomaly, which indicates increased influence of hydrothermal fluids from the open ocean water, probably during the transgression and deposition of the Kamden Member, which is also supported by the high Fe_2O_3 content (> 10 wt-%) (Table S1 in supplementary material). Eventually, the architecture of the CMCP changed from a predominantly steep ramp to a predominantly rimmed margin, which likely limited the influx of open ocean water. Thus, the influence of continental water masses prevailed over the influence of open ocean water, which is visible in the 'continental' REE+Y patterns of the Lyttleton and Eccles carbonates (Fig. 9). However, some samples retained a 'seawater' pattern and even show a slight Eu anomaly, which indicates an occasional influx of open ocean water into the lagoon. REE+Y patterns of slope carbonates (Voegelin et al., 2010) show higher REE+Y values by an order of magnitude and pronounced Eu anomalies as compared to the shelf carbonates, confirming that the slope was mainly influenced by open ocean water. Overall, the influence of different trace element sources (open ocean vs. continental) are supported by the Fe/Mn ratio of carbonates (Eroglu et al., 2015), which confirm that the shift from a dominantly steep ramp, with higher influx of open ocean water to a dominantly rimmed margin architecture, where open ocean influx was limited. Thereby, the draw-down of reducing species from open ocean water (i.e. hydrothermal) influx onto the shallow-water platform might have induced an evolutionary advantage for oxygenic photosynthesis, which is independent from those reduced species (Swanner et al., 2015), and therefore allowed the development of a thriving aerobic ecosystem (e.g. Des Marais, 2001).

5.3. Origin of the mild shift to heavy $\delta^{13}C_{carb}$ signatures in the upper CMCP shelf

Carbonates of the CMCP contain distinct $\delta^{13}C_{carb}$ values, depending on the depositional environment. Carbonates of the very shallow-marine platform facies (KMF-5) reveal an average $\delta^{13}C_{carb}$ signature of -0.38 ± 0.92 (2σ) ‰, and are somewhat isotopically heavier than the carbonates from the stratigraphically correlative lagoonal platform facies of -0.58 ± 0.80 (2σ) ‰ (BH-1) and slope facies of -0.70 ± 1.74 (2σ) ‰ (GKF01) and -0.54 ± 1.22 (2σ) ‰ (GKP01) (Fischer et al., 2009; Horstmann and Beukes, 2002). Thereby, the carbonates of KMF-5 follow an overall trend from bottom to top

from ca. -1.2 ‰ towards heavier isotope signatures of ca. +0.4 ‰ (Fig. 6). The carbonates of BH-1 also adumbrate such a trend from about -1.6 to +0.4 ‰. The deeper slope carbonates from the stratigraphically correlative successions of GKP01 and GKF01 lack this increasing trend but instead vary erratically between about -1.4 to +0.5 ‰, with various excursions to negative values (down to -7.1 ‰) (Fischer et al., 2009). Those excursions represent siderite-rich layers within the slope succession and are connected to the deposition of siliciclastic mudrocks and discrete IF (Fig. 6). All four drill cores exhibit negative excursions related to the deposition of the hematite- and siderite-rich Kamden Member, where GKP01 shows values down to -1.0 ‰, GKF01 down to -7.1 ‰ , BH-1 down to -2.4 ‰ (Fischer et al., 2009), and KMF-5 down to -3.2 ‰. Those negative excursions were likely induced during diagenetic microbial processes such as DIR. Thereby, isotopically light organic material is oxidized to HCO_3^- and Fe(III)-(oxyhydr)oxides reduced to $Fe(II)_{aq}$ in the porewater, where it reacts to isotopically light Fe(II)-carbonate (Fischer et al., 2009; Heimann et al., 2010; Johnson et al., 2008a; Johnson et al., 2008b; Johnson et al., 2008c):

$$4Fe(OH)_3 + CH_2O + 3HCO_3^- \rightarrow 4FeCO_3 + 3OH^- + 7H_2O.$$

Distribution of carbon isotope signatures along the slope and the platform of the CMCP are illustrated in Figure 10, using box and whisker isotopic plots of $\delta^{13}C_{carb}$ data in the single drill cores, distinguishing between the lower CMCP (predominantly steep ramp architecture) and upper CMCP (predominantly rimmed margin architecture). Results reveal some distinct patterns for slope and platform successions. During the deposition of the lower CMCP (Lower Nauga Formation) the slope succession has $\delta^{13}C_{carb}$ mean values (with 2σ) of -0.5 ± 0.6 ‰ (GKP01) and -0.5 ± 0.5 ‰ (GKF01). In the upper CMCP of the slope succession (Upper Nauga Formation), $\delta^{13}C_{carb}$ data (-0.6 ± 1.6 ‰ for GKP01 and -0.6 ± 1.1 ‰ for GKF01) are widely distributed and negative excursions are more frequent. This coincides with the frequent occurrence of mudrock layers in the upper Nauga Formation (Fig. 6), which contained organic carbon that likely fueled DIR-related diagenesis of Fe-(oxyhydr)oxides in the sediment and production of siderite with light $\delta^{13}C_{carb}$ signatures (Fischer et al., 2009; Heimann et al., 2010; Johnson et al., 2008b). The lower CMCP of the shelf succession reveals similar values like the lower slope succession with slightly lighter average $\delta^{13}C_{carb}$ signatures and an overall wider distribution than the upper CMCP, with BH-1 (Reivilo Formation) showing -0.7

± 0.9 ‰ and KMF-5 (Oaktree and Monte Christo formations) showing -0.6 ± 0.9 ‰. The Oaktree and Monte Christo formations (KMF-5) contain mudrocks, which show bulk negative $\delta^{13}C_{carb}$ excursions down to -12.3 ‰ (Fig. S1, supplementary material). This may indicate oxidation of organic matter, however it is unclear whether this signal solely reflects siderite, since the bulk sample was analyzed and no distinctive siderite bands related to the mudrock layers were observed as in the slope succession (Fischer et al., 2009). This implies that DIR processes were probably not as abundant in the platform interior as along the slope, potentially because insufficient Fe-(oxyhydr)oxide was available. The shelf carbonates of the upper CMCP show a different pattern than the Upper Nauga carbonates from the slope facies. The upper CMCP in BH-1 (formations Fairfield to Gamohaan) has a $\delta^{13}C_{carb}$ mean of -0.5 ± 0.6 ‰, no negative excursions and a more narrow distribution (Fig. 10). There is no significant difference between carbonates of GKP01, GKF01, and BH-1 at the 95 % confidence interval (ANOVA, $P > 0.05$). The carbonates of the upper CMCP in KMF-5 (Lyttleton and Eccles formations) on the other hand show a shift in $\delta^{13}C_{carb}$ towards heavier signatures of 0.0 ± 0.5 ‰ (Fig. 10). The difference of KMF-5 to the carbonates of the other three drill cores is significant at the 95 % confidence interval (ANOVA, $P < 0.05$). There are several possible explanations for this shift.

1) The shift could be the result of diagenetic overprint, which seems reasonable considering that this platform experienced early diagenesis in form of dolomitization and silicification. Dolomitization can indeed cause ^{13}C depletion or enrichment and those effects usually overlap (e.g. Irwin et al., 1977; Lyons et al., 1984; Mazzullo, 2000), however this is not mandatory (e.g.Veizer et al., 1989; Veizer et al., 1992). Since the complete Malmani succession was dolomitized, we cannot compare the $\delta^{13}C_{carb}$ signatures of calcitic and dolomitic samples in order to validate this possibility. However, the shelf succession in the Campbellrand Subgroup still contains some calcitic parts. Thus, we evaluated $\delta^{13}C_{carb}$ data of Horstmann and Beukes (2002) and found that calcitic samples ($\delta^{13}C_{carb}$: -0.6 ± 0.9 ‰; n = 29) and dolomitic samples ($\delta^{13}C_{carb}$: -0.6 ± 0.8 ‰; n = 109) show no difference. It seems unlikely that dolomitization caused the shift to heavy $\delta^{13}C_{carb}$ signatures, also because there is no reason why the upper Malmani succession should only be affected and not the lower one, although the complete succession was dolomitized. Silicified carbonates (-0.3 ± 1.2 ‰; n = 37) of the Malmani succession show no relevant difference to unsilicified carbonates (-0.4 ± 0.6 ‰; n = 47). Thus, silicification also

seems unlikely to have induced this shift. However, the fact that silicified carbonates are so abundant in the upper Malmani succession indicates that the same conditions caused for the silicification and the shift to heavier $\delta^{13}C_{carb}$ signatures. Finally, early diagenesis usually leads to a shift to lighter carbon isotope signatures, because degradation of isotopically light organic carbon will affect the isotope signature of carbonate carbon (Veizer et al., 1992), as can be seen in various negative excursions throughout the CMCP (Fischer et al., 2009; Horstmann and Beukes, 2002). Overall, it is unlikely that secondary processes were the reason for the observed mild increase in $\delta^{13}C_{carb}$.

2) Increasing $\delta^{13}C_{carb}$ signatures in the CMCP were reported before and interpreted to reflect a stratified Archean seawater column, where the DIC of deeper seawater interacted with the ocean seafloor and was influenced by hydrothermal input with a lighter isotope signature than the DIC of shallow seawater (Beukes et al., 1990). This model has been questioned, since the light isotope signatures were measured in Fe-rich carbonates, which rather reflect porewater compositions with extreme variable isotope compositions during diagenesis (Fischer et al., 2009; Heimann et al., 2010; Johnson et al., 2008a; Johnson et al., 2008b; Johnson et al., 2008c). Thus, this model of a stratified ocean is an unlikely explanation for the observed shift in $\delta^{13}C_{carb}$.

3) The shift could be the result of increased evaporation on the platform. As we discussed in paragraph 5.1., there are indications, based on evidence of silicification and a shift to heavier $\delta^{13}O_{carb}$ values in the Eccles formation (Fig. S-1) (Burdett et al., 1990; Veizer et al., 1992), that salinity increased over time. Higher salinity conditions are normally a sign of evaporation that would also induce an increase in alkalinity and degassing of CO_2. This can cause a non-equilibrium fractionation of C isotopes and a trend to heavier signatures. However, silicification and the associated shift in $\delta^{13}O_{carb}$ could be related to later diagenetic processes, and do not necessarily record an earlier evaporation process. Alternatively, it has been proposed that an increase in $\delta^{13}C_{carb}$ in modern marine carbonate platforms could be related to the precipitation of increasing proportions of aragonite, which precipitates faster than calcite and is isotopically heavier (~ 2 - 3 ‰ (Romanek et al., 1992)). However, under higher salinity the precipitation rate of aragonite decreases (Zhong and Mucci, 1989). Furthermore, Sumner and Grotzinger (2004) described the in situ precipitation of aragonite along the CMCP also for

subtidal depositional environments and not exclusively for peritidal environments. We doubt that evaporation does explain such a consistent shift in $\delta^{13}C_{carb}$.

4) It is possible that the change in depositional conditions was an important factor for the shift in $\delta^{13}C_{carb}$ signatures, due to the development of a rimmed margin during the deposition of the upper CMCP and the subsequent limited open ocean influx to the platform interior. During earlier stages, the steep ramp architecture allowed for the exposure of the carbonates to open ocean water, which is the largest carbon reservoir in the atmospheric-ocean system (Des Marais, 2001) and would have mainly influenced the $\delta^{13}C$ signatures of the DIC. This is supported by similar mean $\delta^{13}C_{carb}$ signatures and distributions in the lower CMCP of slope and platform carbonates, whereby some negative excursions imply microbial-induced degradation of isotopically light organic matter (Fig. 10). During the rimmed margin stage, the carbonates from the slope facies of the upper CMCP were still exposed to open ocean water and show $\delta^{13}C_{carb}$ distributions similar to the lower CMCP, as well as indications for organic matter degradation. The carbonates from the upper CMCP of the platform facies (Eccles and Lyttleton formations), however, were less exposed to the open ocean water due to the development of the rimmed margin (Beukes, 1987; Sumner and Beukes, 2006) and the restricted conditions probably allowed a distinct development of the DIC pool within the very shallow environment. The organic-rich and siliciclastic mudrocks along the slope facies indicates enhanced primary production in the CMCP and lateral offshore sediment transport of organic material possibly to greater depths and an anoxic milieu (Klein and Beukes, 1989). Such a process would remove isotopically light carbon from the shallow-water lagoon. Since the dominantly rimmed margin architecture limited open ocean influx, it is reasonable to assume that the DIC pool in the shallow-marine environment became slightly more depleted in isotopically light carbon over time.

5.4. Organic carbon content along the CMCP

The lower CMCP, mudrocks and some organic-rich carbonates from the slope reveal mean (with 2σ) TOC contents of 1.61 ± 1.70 wt-% (GKP01) and 1.43 ± 2.52 wt-% (GKF01 – excursion of 9.60 wt-%). In the lower shelf platform (KMF-5) TOC contents are even higher, showing values of 2.73 ± 4.02 wt-%. TOC contents in the upper CMCP show a slight increase in the mean of GKF01 (1.84 ± 2.85

wt-%) and only a negligible decrease in GKP01 (1.52 ± 2.04 wt-%). The platform facies on the other hand shows a strong decline in TOC, coupled with a scarcity of mudrocks (Fig. 6). Several factors are responsible for the preservation of organic matter along shelf and slope of a continental margin, in particular primary production in the euphotic zone (Calvert et al., 1991; Calvert and Pedersen, 1992) and low oxygen concentrations (e.g. Demaison and Moore, 1980; Paropkari et al., 1993). Although a net primary production is obviously necessary, low oxygen concentrations are crucial for the preservation of TOC (Paropkari et al., 1993). Thus, sediments with high TOC content can indicate anoxia, whereas sediments with low TOC content are a sign of oxic conditions. For the CMCP that means that the combination of higher TOC and increase in deposition of mudrocks towards the marginal slope environment indicate a higher burial efficiency of organic matter, which argues for enhanced primary production in the marine environment and anoxic conditions along the platform margin and slope. At the same time, the decrease in TOC in the peritidal environment of the upper CMCP argues for an increase in the oxidation state. In a detailed review of Des Marais (2001) about the carbon cycle during the Precambrian, it is shown that a shift from chemolithoautotrophy and anoxygenic photosynthesis to oxygenic photosynthesis would have induced a significant increase in primary production. This is because chemolithoautotrophy and anoxygenic photosynthesis depend on electron donors like H_2, H_2S, or Fe^{2+} from reduced hydrothermal fluids, and estimates of primary production via those pathways during the Precambrian range from 2 to 20×10^{12} mol/yr C (des Marais, 1985; Turcotte, 1980). Oxygenic photosynthesis is independent of the availability and amount of reduced hydrothermal species and uses H_2O as electron donor, fueling primary productivity (modern rate in marine environment ~ 4000×10^{12} mol/yr C) (Field et al., 1998). Indeed, the development of a rimmed margin and trace element data imply a reduced influx of hydrothermal fluids into the shallow-marine platform interior (Fig. 9). This probably reduced the activity of microorganisms depending on those reduced species and on the other hand allowed oxygenic photosynthesizers to dominate the ecosystem and increase the primary production (Des Marais, 2001). A shift to an aerobic ecosystem would also explain the low amount of organic carbon preserved on the platform facies of the upper CMCP, because the C budget of microbial mats containing cyanobacteria,

is basically steady state in carbon fixation by primary production and carbon loss by heterotrophic respiration (Canfield and des Marais, 1993).

5.5. Isotopic indications for an aerobic ecosystem in the CMCP

Microorganisms kinetically fractionate C and produce organic material with very light $\delta^{13}C$ signatures that vary, depending on the metabolic pathway (Figs. 5, 7) (e.g. Hayes, 2001; Zerkle et al., 2005). Most of the carbonate and mudrock samples from the CMCP show signatures between -40 and -20 ‰. Slope carbonates of the Lower and Upper Nauga formations show mean $\delta^{13}C_{org}$ signatures (with 2σ) of -31.5 ± 3.16 ‰ (GKP01) and -31.5 ± 4.0 ‰ (GKF01) (Fischer et al., 2009; Horstmann and Beukes, 2002). Lagoonal carbonates show a mean of -30.2 ± 5.0 ‰ (BH-1), while peritidal carbonates (KMF-5) reveal a shift to heavier signatures (-25.8 ± 5.2 ‰) (Tables S3, S4 in supplementary material), although few carbonates might be altered and do not record pristine values. Nevertheless, most carbonate signatures of organic material from the peritidal environment up to ~-25 ‰ still show a disordered structure and low carbonization (Figs. 2, 5), which indicate that an original isotope ratio was preserved and recorded a different ecosystem in the very shallow-marine environment. Assuming a marine DIC pool with a $\delta^{13}C$ signature of ~ 0 ‰, oxygenic photoautotrophy (e.g., by cyanobacteria) would typically yield $\delta^{13}C_{org}$ signatures between -33 to -24 ‰, although those signatures can also be produced by some anaerobic bacteria such as photoferroautotrophic, sulfate-reducing, methanogenic and even methanotrophic bacteria (Thomazo et al., 2009 and references therein) (Fig. 6). However, evidence for dissolved oxygen in the shallow seawater of the Campbellrand-Malmani area, such as authigenic accumulation of redox-sensitive elements and the enrichment of carbonates and mudrocks in heavy stable molybdenum and nitrogen isotopes (Godfrey and Falkowski, 2009; Voegelin et al., 2010; Wille et al., 2007 and this study) support the existence of oxygenic photoautotrophs in marine microbial mats. This is supported by the slightly heavier $\delta^{13}C_{carb}$ signatures in the restricted platform facies that argue for an increasing oxidation state in the shallow-marine environment. Diminished ferrous iron delivery to shallow water, as indicated by trace element systematics and depth variant Fe concentrations of the carbonates (Fig. 8, 9) (Eroglu et al., 2015), would have favored enhanced activity of cyanobacteria, which are susceptible to ferrous iron toxicity (Swanner et al., 2015) and would have

restricted the activity of ferrous anoxygenic phototrophs. Mudrocks from the slope toward the shallow-water platform show a mean $\delta^{13}C_{org}$ value of ~-32 ‰ (Fig. 10), which could indicate preserved photosynthetic mass. However, some negative excursions down to -40 ‰ and below (Fig. 6) argue for methane cycling or sulfate-reduction by an anaerobic microbial community within reducing sediments. Overall, $\delta^{13}C_{org}$ isotope signatures of carbonates along the CMCP show a dominance of photoautotrophic bacteria and heterotrophic respiration of the photosynthetic biomass, with the possibility of locally occurring anaerobic microbial activity in some mudrock layers. Despite the possibility that some of these signatures might have been slightly shifted due to higher peak metamorphic temperatures, as indicated by Raman analyses (Table S5 in supplementary material, Fig. 2 and 5), the range in $\delta^{13}C_{org}$ from ~ -40 ‰ in mudrocks to up to ~ -25 ‰ in peritidal carbonates cannot be explained by metamorphic overprinting but rather supports a diverse ecosystem with a dominance of aerobic ecosystems in the platform's shallow waters. This is consistent with data from other Archean carbonate successions of Steep Rock (2.8 Ga, Canada) (Grassineau et al., 2006) and Hamersley Basin (2.6 Ga, Australia) (Eigenbrode and Freeman, 2006), which also contain sediments with similarly varying $\delta^{13}C_{org}$ values that point to a change from anaerobic to enhanced aerobic microbial activity on consolidated shallow marine platforms.

6. CONCLUSIONS

This study provides a complete reconstruction of the evolution of an inferred oxygen oasis, here represented by the Campbellrand-Malmani carbonate platform (CMCP) about 200 Ma before the GOE, based on trace element signatures. It confirms earlier findings, which proposed that the architecture and orientation of carbonate platforms provided microbial ecosystem protection from the anoxic open ocean and allowed the development of an aerobic ecosystem (Des Marais, 2001; Eigenbrode and Freeman, 2006; Riding et al., 2014). Deposition of siliciclastic and organic-rich mudrocks dynamically changes over time in the CMCP. In the lower CMCP, mudrocks are abundant in the shallow-marine platform, while in the upper CMCP mudrocks are scarce on the platform interior, but still accumulate along the slope. This possibly indicates increases in the primary production, in the efficiency of organic burial along the anoxic margin, and in the oxidation state in

the platform interior. While enhanced organic matter production and oxygen produced by photosynthesis is one requirement for oxygen accumulation, another one is a decrease of reducing species. We propose that this is induced by the development of a rimmed margin, which limited the influx of reducing waters from the open ocean. A mild shift to heavier $\delta^{13}C_{carb}$ values on the platform facies of the upper CMCP compared to the slope facies supports a continued removal of isotopically light carbon from the system and an increase in the isotope signature of the lagoonal DIC pool. We propose that a shift in the isotopic composition of the dissolved inorganic carbon pool is another important proxy for Precambrian oxygen oases, in particular combined with $\delta^{13}C_{org}$ data indicating a shift from an anaerobic to an aerobic biosphere on the platform.

REFERENCES

Allan, J.R., Matthews, R.K., 1982. Isotope Signatures Associated with Early Meteoric Diagenesis. Sedimentology 29, 797-817.

Allwood, A.C., Kamber, B.S., Walter, M.R., Burch, I.W., Kanik, I., 2010. Trace elements record depositional history of an Early Archean stromatolitic carbonate platform. Chem Geol 270, 148-163.

Altermann, W., Siegfried, H.P., 1997. Sedimentology and facies development of an Archaean shelf: carbonate platform transition in the Kaapvaal Craton, as deduced from a deep borehole at Kathu, South Africa. J Afr Earth Sci 24, 391-410.

Anbar, A.D., Duan, Y., Lyons, T.W., Arnold, G.L., Kendall, B., Creaser, R.A., Kaufman, A.J., Gordon, G.W., Scott, C., Garvin, J., Buick, R., 2007. A whiff of oxygen before the Great Oxidation Event? Science 317, 1903-1906.

Banner, J.L., 1995. Application of the Trace-Element and Isotope Geochemistry of Strontium to Studies of Carbonate Diagenesis. Sedimentology 42, 805-824.

Bau, M., 1999. Scavenging of dissolved yttrium and rare earths by precipitating iron oxyhydroxide: Experimental evidence for Ce oxidation, Y-Ho fractionation, and lanthanide tetrad effect. Geochim Cosmochim Ac 63, 67-77.

Bau, M., Dulski, P., 1999. Comparing yttrium and rare earths in hydrothermal fluids from the Mid-Atlantic Ridge: implications for Y and REE behaviour during near-vent mixing and for the Y/Ho ratio of Proterozoic seawater. Chem Geol 155, 77-90.

Bekker, A., Holland, H.D., Wang, P.L., Rumble, D., Stein, H.J., Hannah, J.L., Coetzee, L.L., Beukes, N.J., 2004. Dating the rise of atmospheric oxygen. Geochim Cosmochim Ac 68, A780-A780.

Beukes, N.J., 1987. Facies Relations, Depositional-Environments and Diagenesis in a Major Early Proterozoic Stromatolitic Carbonate Platform to Basinal Sequence, Campbellrand Subgroup, Transvaal Supergroup, Southern-Africa. Sediment Geol 54, 1-46.

Beukes, N.J., Gutzmer, J., 2008. Origin and paleoenvironmental significance of major iron formations at the Archean-Paleoproterozoic Boundary. Society of Economic Geologists 15, 5-47.

Beukes, N.J., Klein, C., Kaufman, A.J., Hayes, J.M., 1990. Carbonate Petrography, Kerogen Distribution, and Carbon and Oxygen Isotope Variations in an Early Proterozoic Transition from Limestone to Iron-Formation Deposition, Transvaal Supergroup, South-Africa. Econ Geol Bull Soc 85, 663-690.

Beyssac, O., Bollinger, L., Avouac, J.P., Goffe, B., 2004. Thermal metamorphism in the lesser Himalaya of Nepal determined from Raman spectroscopy of carbonaceous material. Earth Planet Sc Lett 225, 233-241.

Beyssac, O., Goffe, B., Chopin, C., Rouzaud, J.N., 2002. Raman spectra of carbonaceous material in metasediments: a new geothermometer. J Metamorph Geol 20, 859-871.

Brand, U., Veizer, J., 1980. Chemical Diagenesis of a Multicomponent Carbonate System .1. Trace-Elements. Journal of Sedimentary Petrology 50, 1219-1236.

Brocks, J.J., 2011. Millimeter-scale concentration gradients of hydrocarbons in Archean shales: Live-oil escape or fingerprint of contamination? Geochim Cosmochim Ac 75, 3196-3213.

Brocks, J.J., Logan, G.A., Buick, R., Summons, R.E., 1999. Archean molecular fossils and the early rise of eukaryotes. Science 285, 1033-1036.

Buick, I.S., Maas, R., Gibson, R., 2001. Precise U-Pb titanite age constraints on the emplacement of the Bushveld Complex, South Africa. J Geol Soc London 158, 3-6.

Burdett, J.W., Grotzinger, J.P., Arthur, M.A., 1990. Did Major Changes in the Stable-Isotope Composition of Proterozoic Seawater Occur. Geology 18, 227-230.

Button, A., 1973. The stratigraphic history of the Malmani Dolomite in the eastern and north-eastern Transvaal. Transactions of the Geological Society of South Africa 76, 229-247.

Calvert, S.E., Karlin, R.E., Toolin, L.J., Donahue, D.J., Southon, J.R., Vogel, J.S., 1991. Low Organic-Carbon Accumulation Rates in Black-Sea Sediments. Nature 350, 692-695.

Calvert, S.E., Pedersen, T.F., 1992. Organic carbon accumulation and preservation in marine sediments: how important is anoxia?, in: Whelan, J., Farrington, J.W. (Eds.), Organic matter: productivity, accumulation, and preservation in recent and ancient sediments. Columbia University Press, New York, pp. 231-263.

Canfield, D.E., des Marais, D.J., 1993. Biogeochemical Cycles of Carbon, Sulfur, and Free Oxygen in a Microbial Mat. Geochim Cosmochim Ac 57, 3971-3984.

Chakrabarti, R., Knoll, A.H., Jacobsen, S.B., Fischer, W.W., 2012. Si isotope variability in Proterozoic cherts. Geochim Cosmochim Ac 91, 187-201.

Craig, H., 1957. Isotopic standards for carbon and oxygen and correction factors for mass spectrometric analysis of carbon dioxide. Geochim Cosmochim Ac 12, 133-149.

Crne, A.E., Melezhik, V.A., Lepland, A., Fallick, A.E., Prave, A.R., Brasier, A.T., 2014. Petrography and geochemistry of carbonate rocks of the Paleoproterozoic Zaonega Formation, Russia: Documentation of C-13-depleted non-primary calcite. Precambrian Res 240, 79-93.

Crowe, S.A., Dossing, L.N., Beukes, N.J., Bau, M., Kruger, S.J., Frei, R., Canfield, D.E., 2013. Atmospheric oxygenation three billion years ago. Nature 501, 535-+.

De la Rocha, C.L., Brzezinski, M.A., DeNiro, M.J., 2000. A first look at the distribution of the stable isotopes of silicon in natural waters. Geochim Cosmochim Ac 64, 2467-2477.

Delarue, F., Rouzaud, J.N., Derenne, S., Bourbin, M., Westall, F., Kremer, B., Sugitani, K., Deldicque, D., Robert, F., 2016. The Raman-Derived Carbonization Continuum: A Tool to Select the Best Preserved Molecular Structures in Archean Kerogens. Astrobiology 16, 407-417.

Demaison, G.J., Moore, G.T., 1980. Anoxic Environments and Oil Source Bed Genesis. Aapg Bull 64, 1179-1209.

Derry, L.A., 2010a. A burial diagenesis origin for the Ediacaran Shuram-Wonoka carbon isotope anomaly. Earth Planet Sc Lett 294, 152-162.

Derry, L.A., 2010b. On the significance of delta C-13 correlations in ancient sediments. Earth Planet Sc Lett 296, 497-501.

Derry, L.A., Jacobsen, S.B., 1990. The Chemical Evolution of Precambrian Seawater - Evidence from Rees in Banded Iron Formations. Geochim Cosmochim Ac 54, 2965-2977.

des Marais, D.J., 1985. Carbon exchange between the mantle and crust and its effect upon the atmosphere: today compared to Archean time, in: Sundquist, E.T., Broecker, W.S. (Eds.), The Carbon Cycle and Atmospheric CO2: Natural Variations Archean to Present. American Geophysical Union, Washington, D.C., pp. 605-611.

Des Marais, D.J., 2001. Isotopic evolution of the biogeochemical carbon cycle during the Precambrian, in: Valley, J.W., Cole, D.R. (Eds.), Stable Isotope Geochemistry. Reviews in Mineralogy and Geochemistry, pp. 555-578.

Duan, Y., Anbar, A.D., Arnold, G.L., Lyons, T.W., Gordon, G.W., Kendall, B., 2010. Molybdenum isotope evidence for mild environmental oxygenation before the Great Oxidation Event. Geochim Cosmochim Ac 74, 6655-6668.

Duan, Y., Arnold, G.L., Gordon, G.W., Anbar, A.D., 2008. Evidence from Mo isotopic compositions for "A whiff of oxygen" before the Great Oxidation Event. Geochim Cosmochim Ac 72, A228-A228.

Eigenbrode, J.L., Freeman, K.H., 2006. Late Archean rise of aerobic microbial ecosystems. P Natl Acad Sci USA 103, 15759-15764.

Eigenbrode, J.L., Freeman, K.H., Summons, R.E., 2008. Methylhopane biomarker hydrocarbons in Hamersley Province sediments provide evidence for Neoarchean aerobiosis. Earth Planet Sc Lett 273, 323-331.

Eroglu, S., Schoenberg, R., Wille, M., Beukes, N., Taubald, H., 2015. Geochemical stratigraphy, sedimentology, and Mo isotope systematics of the ca. 2.58-2.50 Ga-old Transvaal Supergroup carbonate platform, South Africa. Precambrian Res 266, 27-46.

Falkowski, P.G., Isozaki, Y., 2008. Geology - The story of O(2). Science 322, 540-542.

Farquhar, J., Bao, H.M., Thiemens, M., 2000. Atmospheric influence of Earth's earliest sulfur cycle. Science 289, 756-758.

Field, C.B., Behrenfeld, M.J., Randerson, J.T., Falkowski, P., 1998. Primary production of the biosphere: Integrating terrestrial and oceanic components. Science 281, 237-240.

Fischer, A.G., 1965. Fossils Early Life and Atmospheric History. P Natl Acad Sci USA 53, 1205-&.

Fischer, W.W., Schröder, S., Lacassie, J.P., Beukes, N.J., Goldberg, T., Strauss, H., Horstmann, U.E., Schrag, D.P., Knoll, A.H., 2009. Isotopic constraints on the Late Archean carbon cycle from the Transvaal Supergroup along the western margin of the Kaapvaal Craton, South Africa. Precambrian Res 169, 15-27.

Folk, R.L., Land, L.S., 1975. Mg/Ca Ratio and Salinity - 2 Controls over Crystallization of Dolomite. Aapg Bull 59, 60-68.

Foucher, F., Ammar, M.R., Westall, F., 2015. Revealing the biotic origin of silicified Precambrian carbonaceous microstructures using Raman spectroscopic mapping, a potential method for the detection of microfossils on Mars. J Raman Spectrosc 46, 873-879.

Frauenstein, F., Veizer, J., Beukes, N., Van Niekerk, H.S., Coetzee, L.L., 2009. Transvaal Supergroup carbonates: Implications for Paleoproterozoic delta O-18 and delta C-13 records. Precambrian Res 175, 149-160.

Freeman, K.H., Hayes, J.M., Trendel, J.M., Albrecht, P., 1990. Evidence from Carbon Isotope Measurements for Diverse Origins of Sedimentary Hydrocarbons. Nature 343, 254-256.

Frei, R., Gaucher, C., Poulton, S.W., Canfield, D.E., 2009. Fluctuations in Precambrian atmospheric oxygenation recorded by chromium isotopes. Nature 461, 250-U125.

French, K.L., Hallmann, C., Hope, J.M., Schoon, P.L., Zumberge, J.A., Hoshino, Y., Peters, C.A., George, S.C., Love, G.D., Brocks, J.J., Buick, R., Summons, R.E., 2015. Reappraisal of hydrocarbon biomarkers in Archean rocks. P Natl Acad Sci USA 112, 5915-5920.

Georg, R.B., Reynolds, B.C., West, A.J., Burton, K.W., Halliday, A.N., 2007. Silicon isotope variations accompanying basalt weathering in Iceland. Earth Planet Sc Lett 261, 476-490.

Godfrey, L.V., Falkowski, P.G., 2009. The cycling and redox state of nitrogen in the Archaean ocean. Nat Geosci 2, 725-729.

Grassineau, N.V., Abell, P., Appel, P.W.U., Lowry, D., Nisbet, E.G., 2006. Early life signatures in sulfur and carbon isotopes from Isua, Barberton, Wabigoon (Steep Rock), and Belingwe Greenstone Belts (3.8 to 2.7 Ga) in: Kesler, S.E., Ohmoto, H. (Eds.), Evolution of Early Earth's Atmosphere, Hydrosphere, and Biosphere - Constraints from Ore Deposits. Geological Society of America Memoirs, pp. 33-52.

Grotzinger, J.P., 1989. Facies and evolution of Precambrian carbonate depositional systems: emergence of the modern platform archetype, in: Crevello, P.D., Wilson, J.L., Sarg, J.F., Read, J.F. (Eds.), Controls on Carbonate Platform and Basin Development. SEPM Special Publication, pp. 79-106.

Gumsley, A.P., Chamberlain, K.R., Bleeker, W., Soderlund, U., Kock, M.D.O., Larsson, E.R., Bekker, A., 2017. Timing and tempo of the Great Oxidation Event. P Natl Acad Sci USA 114, 1811-1816.

Hannah, J.L., Bekker, A., Stein, H.J., Markey, R.J., Holland, H.D., 2004. Primitive Os and 2316 Ma age for marine shale: implications for Paleoproterozoic glacial events and the rise of atmospheric oxygen. Earth Planet Sc Lett 225, 43-52.

Hayes, J.M., 2001. Fractionation of carbon and hydrogen isotopes in biosynthetic processes, in: Valley, J.W., Cole, D.R. (Eds.), Stable Isotope Geochemistry. Mineralogical Society of America, Washington, D.C., pp. 225-278.

Heimann, A., Johnson, C.M., Beard, B.L., Valley, J.W., Roden, E.E., Spicuzza, M.J., Beukes, N.J., 2010. Fe, C, and O isotope compositions of banded iron formation carbonates demonstrate a major role for dissimilatory iron reduction in similar to 2.5 Ga marine environments. Earth Planet Sc Lett 294, 8-18.

Herman, E.K., Kump, L.R., 2005. Biogeochemistry of microbial mats under Precambrian environmental conditions: a modelling study. Geobiology 3, 77-92.

Hoffman, P., 1988. Pethei reef complex (1.9 Ga), Great Slave Lake, NWT, in: Geldsetzer, H.H.J., James, N.P., Tebbutt, G.E. (Eds.), Reefs, Canada and Adjacent Areas, Canadian Society of Petroleum Geologists Memoir pp. 38-48.

Hoffman, P., Grotzinger, J., 1988. Abner/Denault Reef Complex (2.1 Ga), Labrador Trough, NE Quebec, in: Geldsetzer, H.H.J., James, N.P., Tebbutt, G.E. (Eds.), Reefs, Canada and Adjacent Areas. Canadian Society of Petroleum Geologists Memoir pp. 49-54.

Holmden, C., Creaser, R.A., Muehlenbachs, K., Leslie, S.A., Bergstrom, S.M., 1998. Isotopic evidence for geochemical decoupling between ancient epeiric seas and bordering oceans: Implications for secular curves. Geology 26, 567-570.

Horstmann, U.E., Beukes, N.J., 2002. Stable isotope geochemistry of the Campbellrand Dolomite in the SACHA drill core. Collaborative project with SA universities, Department of Geology, Rand Afrikaans University , Report Stable Isotope Lab 2001-06.

Immenhauser, A., Della Porta, G., Kenter, J.A.M., Bahamonde, J.R., 2003. An alternative model for positive shifts in shallow-marine carbonate delta C-13 and delta O-18. Sedimentology 50, 953-959.

Irwin, H., Curtis, C., Coleman, M., 1977. Isotopic Evidence for Source of Diagenetic Carbonates Formed during Burial of Organic-Rich Sediments. Nature 269, 209-213.

Jiang, G.Q., Wang, X.Q., Shi, X.Y., Xiao, S.H., Zhang, S.H., Dong, J., 2012. The origin of decoupled carbonate and organic carbon isotope signatures in the early Cambrian (ca. 542-520 Ma) Yangtze platform. Earth Planet Sc Lett 317, 96-110.

Johnson, C., Beard, B., Roden, E., 2008a. Temporal variations in Fe isotope compositions of banded iron formations record changes in the nature of redox cycling. Geochim Cosmochim Ac 72, A435-A435.

Johnson, C.M., Beard, B.L., Klein, C., Beukes, N.J., Roden, E.E., 2008b. Iron isotopes constrain biologic and abiologic processes in banded iron formation genesis. Geochim Cosmochim Ac 72, 151-169.

Johnson, C.M., Beard, B.L., Roden, E.E., 2008c. The iron isotope fingerprints of redox and biogeochemical cycling in the modern and ancient Earth. Annu Rev Earth Pl Sc 36, 457-493.

Kamber, B.S., Bolhar, R., Webb, G.E., 2004. Geochemistry of late Archaean stromatolites from Zimbabwe: evidence for microbial life in restricted epicontinental seas. Precambrian Res 132, 379-399.

Kamber, B.S., Webb, G.E., 2001. The geochemistry of late Archaean microbial carbonate: Implications for ocean chemistry and continental erosion history. Geochim Cosmochim Ac 65, 2509-2525.

Kasting, J.F., 1991. Box models for the evolution of atmospheric oxygen: an update. Palaeogeogr Palaeocl 97, 125-131.

Kasting, J.F., 1992. Models relating to Proterozoic atmospheric and ocean chemistry, in: Schopf, J., Klein, C. (Eds.), The Proterozoic Biosphere, A Multidisciplinary Study. Cambridge University Press, Cambridge, pp. 1185-1187.

Kasting, J.F., Howard, M.T., Wallmann, K., Veizer, J., Shields, G., Jaffres, J., 2006. Paleoclimates, ocean depth, and the oxygen isotopic composition of seawater. Earth Planet Sc Lett 252, 82-93.

Kasting, J.F., Siefert, J.L., 2002. Life and the evolution of Earth's atmosphere. Science 296, 1066-1068.

Kendall, B., Reinhard, C.T., Lyons, T., Kaufman, A.J., Poulton, S.W., Anbar, A.D., 2010. Pervasive oxygenation along late Archaean ocean margins. Nat Geosci 3, 647-652.

Klein, C., Beukes, N.J., 1989. Geochemistry and Sedimentology of a Facies Transition from Limestone to Iron-Formation Deposition in the Early Proterozoic Transvaal Supergroup, South-Africa. Econ Geol 84, 1733-1774.

Knauth, L.P., 1979. Model for the Origin of Chert in Limestone. Geology 7, 274-277.

Knoll, A.H., 1985. Exceptional Preservation of Photosynthetic Organisms in Silicified Carbonates and Silicified Peats. Philos T Roy Soc B 311, 111-&.

Knoll, A.H., Beukes, N.J., 2009. Introduction: Initial investigations of a Neoarchean shelf margin-basin transition (Transvaal Supergroup, South Africa). Precambrian Res 169, 1-14.

Kohout, F.A., 1967. Groundwater flow and the geothermal regime of the Floridan plateau. Trans. Gulf-Cst. Ass. Geol. Socs. 17, 339-354.

Kretz, R., 1982. A Model for the Distribution of Trace-Elements between Calcite and Dolomite. Geochim Cosmochim Ac 46, 1979-1981.

Kump, L.R., Barley, M.E., 2007. Increased subaerial volcanism and the rise of atmospheric oxygen 2.5 billion years ago. Nature 448, 1033-1036.

Kurzweil, F., Wille, M., Schoenberg, R., Taubald, H., Van Kranendonk, M.J., 2015. Continuously increasing delta Mo-98 values in Neoarchean black shales and iron formations from the Hamersley Basin. Geochim Cosmochim Ac 164, 523-542.

Lahfid, A., Beyssac, O., Deville, E., Negro, F., Chopin, C., Goffe, B., 2010. Evolution of the Raman spectrum of carbonaceous material in low-grade metasediments of the Glarus Alps (Switzerland). Terra Nova 22, 354-360.

Lalonde, S.V., Konhauser, K.O., 2015. Benthic perspective on Earth's oldest evidence for oxygenic photosynthesis. P Natl Acad Sci USA 112, 995-1000.

Land, L.S., 1985. The Origin of Massive Dolomite. J Geol Educ 33, 112-125.

Lawrence, M.G., Kamber, B.S., 2006. The behaviour of the rare earth elements during estuarine mixing-revisited. Mar Chem 100, 147-161.

Lippmann, F., 1973. Sedimentary Carbonate Minerals. Springer-Verlag, berlin.

Luo, G., Ono, S., Beukes, N.J., Wang, D.T., Xie, S., Summons, R.E., 2016. Rapid oxygenation of Earth's atmosphere 2.33 billion years ago. Science Advances 2.

Lyons, W.B., Long, D.T., Hines, M.E., Gaudette, H.E., Armstrong, P.B., 1984. Calcification of Cyanobacterial Mats in Solar Lake, Sinai. Geology 12, 623-626.

Maier, W.D., Barnes, S.J., 1998. Concentrations of rare earth elements in silicate rocks of the Lower, Critical and Main Zones of the Bushveld Complex. Chem Geol 150, 85-103.

Maliva, R.G., Siever, R., 1988. Pre-Cenozoic Nodular Cherts - Evidence for Opal-Ct Precursors and Direct Quartz Replacement. Am J Sci 288, 798-809.

Maliva, R.G., Siever, R., 1989. Nodular Chert Formation in Carbonate Rocks. J Geol 97, 421-433.

Marx, S.K., Kamber, B.S., 2010. High-precision trace-element systematics of sediments in the Murray-Darling Basin, Australia: Sediment tracing and palaeo-climate implications of fine scale chemical heterogeneity of the upper continental crust. Applied Geochemistry 25, 1221-1237.

Mazzullo, S.J., 2000. Organogenic dolomitization in peritidal to deep-sea sediments. J Sediment Res 70, 10-23.

Mcneill, D.F., Kirschvink, J.L., 1993. Early Dolomitization of Platform Carbonates and the Preservation of Magnetic Polarity. J Geophys Res-Sol Ea 98, 7977-7986.

Miyano, T., Beukes, N.J., 1984. Phase relations of stilpnomelane, ferriannite, and riebeckite in very low-grade metamorphosed iron-formations. Transactions of the Geological Society of South Africa 87, 111-124.

Morrow, D.W., 1982. Diagenesis 1: Dolomite - Part 1, the chemistry of dolomitization and dolomite precipitation. Geoscience Canada 9, 5-13.

Murray, R.C., 1960. The origin of porosity in carbonate rocks. Journal of Sedimentary Petrology 30, 59-84.

Nisbet, E.G., Sleep, N.H., 2001. The habitat and nature of early life. Nature 409, 1083-1091.

Oehlert, A.M., Swart, P.K., 2014. Interpreting carbonate and organic carbon isotope covariance in the sedimentary record. Nat Commun 5.

Olcott-Marshall, A., Emry, J.R., Marshall, C.P., 2012. Multiple Generations of Carbon in the Apex Chert and Implications for Preservation of Microfossils. Astrobiology 12, 160-166.

Olson, S.L., Kump, L.R., Kasting, J.F., 2013. Quantifying the areal extent and dissolved oxygen concentrations of Archean oxygen oases. Chem Geol 362, 35-43.

Paropkari, A.L., Babu, C.P., Mascarenhas, A., 1993. New Evidence for Enhanced Preservation of Organic-Carbon in Contact with Oxygen Minimum Zone on the Western Continental-Slope of India. Mar Geol 111, 7-13.

Pavlov, A.A., Kasting, J.F., 2002. Mass-independent fractionation of sulfur isotopes in Archean sediments: Strong evidence for an anoxic Archean atmosphere. Astrobiology 2, 27-41.

Pearce, J.A., 1983. Role of the sub-continental lithosphere in magma genesis at active continental margins, in: Hawkesworth, C.J., Norry, M.J. (Eds.), Continental Basalts and Mantle Xenoliths. Shiva Press, Nantwich, U.K., pp. 230-249.

Planavsky, N.J., Asael, D., Hofmann, A., Reinhard, C.T., Lalonde, S.V., Knudsen, A., Wang, X.L., Ossa, F.O., Pecoits, E., Smith, A.J.B., Beukes, N.J., Bekker, A., Johnson, T.M., Konhauser, K.O., Lyons, T.W., Rouxel, O.J., 2014. Evidence for oxygenic photosynthesis half a billiion years before the Great Oxidation Event. Nat Geosci 7, 283-286.

Purser, B., Tucker, M.E., Zenger, D., 21. , . 1994. Dolomites: A Volume in Honour of Dolomieu. Blackwell Science, Oxford.

Reeder, R., 1983. Crystal chemistry of the rhombohedral carbonates, in: Reeder, R. (Ed.), Carbonates: Mineralogy and Chemisty. Bookcrafters, Chelsea, pp. 1-47.

Reinhard, C.T., Lalonde, S.V., Lyons, T.W., 2013. Oxidative sulfide dissolution on the early Earth. Chem Geol 362, 44-55.

Riding, R., Fralick, P., Liang, L.Y., 2014. Identification of an Archean marine oxygen oasis. Precambrian Res 251, 232-237.

Robinson, J.J., Scott, K.M., Swanson, S.T., O'Leary, M.H., Horken, K., Tabita, F.R., Cavanaugh, C.M., 2003. Kinetic isotope effect and characterization of form II RubisCO from the chemoautotrophic endosymbionts of the hydrothermal vent tubeworm Riftia pachyptila. Limnol Oceanogr 48, 48-54.

Romanek, C.S., Grossman, E.L., Morse, J.W., 1992. Carbon Isotopic Fractionation in Synthetic Aragonite and Calcite - Effects of Temperature and Precipitation Rate. Geochim Cosmochim Ac 56, 419-430.

Rouzaud, J.N., Deldicque, D., Charon, E., Pageot, J., 2015. Carbons at the heart of questions on energy and environment: A nanostructural approach. Cr Geosci 347, 124-133.

Schröder, S., Lacassie, J.P., Beukes, N.J., 2006. Stratigraphic and geochemical framework of the Agouron drill cores, Transvaal Supergroup (Neoarchean-Paleoproterozoic, South Africa). S Afr J Geol 109, 23-54.

Scott, K.M., Schwedock, J., Schrag, D.P., Cavanaugh, C.M., 2004. Influence of form IA RubisCO and environmental dissolved inorganic carbon on the delta C-13 of the clam-chemoautotroph symbiosis Solemya velum. Environ Microbiol 6, 1210-1219.

Seto, M., Akagi, T., 2008. Chemical condition for the appearance of a negative Ce anomaly in stream waters and groundwaters. Geochem J 42, 371-380.

Sforna, M.C., van Zuilen, M.A., Philippot, P., 2014. Structural characterization by Raman hyperspectral mapping of organic carbon in the 3.46 billion-year-old Apex chert, Western Australia. Geochim Cosmochim Ac 124, 18-33.

Shields, G., Veizer, J., 2002. Precambrian marine carbonate isotope database: Version 1.1. Geochem Geophy Geosy 3.

Siever, R., 1962. Silica Solubility, 0-Degrees-C-200-Degrees-C, and the Diagenesis of Siliceous Sediments. J Geol 70, 127-150.

Simms, M., 1984. Dolomitization by Groundwater-Flow Systems in Carbonate Platforms. Aapg Bull 68, 1219-1220.

Sirevag, R., 1995. Carbon metabolism in green bacteria, in: Blankenship, R.E., Madigan, M.T., Bauer, C.E. (Eds.), Anoxygenic Photosynthetic Bacteria: Advances in Photosynthesis, Dordrecht, pp. 871-883.

Sumner, D., 2002. Neoarchean Carbonates - Clues to Early Life and Early Ocean Chemistry, 16th International Sedimentological Congress. International Association of Sedimentologists, Rand Afrikaans University - Johannesburg, South Africa.

Sumner, D.Y., Beukes, N.J., 2006. Sequence stratigraphic development of the Neoarchean Transvaal carbonate platform, Kaapvaal Craton, South Africa. S Afr J Geol 109, 11-22.

Sumner, D.Y., Grotzinger, J.P., 1996. Were kinetics of Archean calcium carbonate precipitation related to oxygen concentration? Geology 24, 119-122.

Sumner, D.Y., Grotzinger, J.P., 2004. Implications for Neoarchaean ocean chemistry from primary carbonate mineralogy of the Campbellrand-Malmani Platform, South Africa. Sedimentology 51, 1273-1299.

Sumner, D.Y., Hawes, I., Mackey, T.J., Jungblut, A.D., Doran, P.T., 2015. Antarctic microbial mats: A modern analog for Archean lacustrine oxygen oases. Geology 43, 887-890.

Swanner, E.D., Mloszewska, A.M., Cirpka, O.A., Schoenberg, R., Konhauser, K.O., Kappler, A., 2015. Modulation of oxygen production in Archaean oceans by episodes of Fe(II) toxicity. Nat Geosci 8, 126-130.

Swart, P.K., Ruiz, J., Holmes, C.W., 1987. Use of Strontium Isotopes to Constrain the Timing and Mode of Dolomitization of Upper Cenozoic Sediments in a Core from San Salvador, Bahamas. Geology 15, 262-265.

Tabita, F.R., 1999. Microbial ribulose 1,5-bisphosphate carboxylase/oxygenase: A different perspective. Photosynth Res 60, 1-28.

Taylor, S.R., MacLennan, S.H., 1985. The Continental Crust: Its Composition and Evolution. Blackwell, Oxford.

Thomazo, C., Pinti, D.L., Busigny, V., Ader, M., Hashizume, K., Philippot, P., 2009. Biological activity and the Earth's surface evolution: Insights from carbon, sulfur, nitrogen and iron stable isotopes in the rock record. Cr Palevol 8, 665-678.

Turcotte, D.L., 1980. On the Thermal Evolution of the Earth. Earth Planet Sc Lett 48, 53-58.

Valentine, D.L., Chidthaisong, A., Rice, A., Reeburgh, W.S., Tyler, S.C., 2004. Carbon and hydrogen isotope fractionation by moderately thermophilic methanogens. Geochim Cosmochim Ac 68, 1571-1590.

Valley, J.W., 1986. Stable isotope geochemistry of metamorphic rocks, in: Valley, J.W., Taylor, H.P., O'Neil, J.R. (Eds.), Stable Iso-topes in High Temperature Geological Pro-cesses. Mineralogical Society of America, pp. 445-498.

Valley, J.W., O'Neil, J.R., 1981. C-13-C-12 Exchange between Calcite and Graphite - a Possible Thermometer in Grenville Marbles. Geochim Cosmochim Ac 45, 411-419.

van den Boorn, S.H.J.M., 2008. Silicon isotopes and the origin of Archaean cherts. University of Utrecht, p. 277.

Veizer, J., 1983. Chemical diagenesis of carbonates: theory and application of trace element techniques, in: Arthur, M.A., Anderson, T.F., Kaplan, I.R., Veizer, J., Land, L.S. (Eds.), Stable Isotopes in Sedimentary Geology. Society of Economic Paleontologists and Mineralogists Short Course Notes, pp. III-1-III-100.

Veizer, J., Ala, D., Azmy, K., Bruckschen, P., Buhl, D., Bruhn, F., Carden, G.A.F., Diener, A., Ebneth, S., Godderis, Y., Jasper, T., Korte, C., Pawellek, F., Podlaha, O.G., Strauss, H., 1999. Sr-87/Sr-86, delta C-13 and delta O-18 evolution of Phanerozoic seawater. Chem Geol 161, 59-88.

Veizer, J., Hoefs, J., Lowe, D.R., Thurston, P.C., 1989. Geochemistry of Precambrian Carbonates .2. Archean Greenstone Belts and Archean Sea-Water. Geochim Cosmochim Ac 53, 859-871.

Veizer, J., Plumb, K.A., Clayton, R.N., Hinton, R.W., Grotzinger, J.P., 1992. Geochemistry of Precambrian Carbonates .5. Late Paleoproterozoic Seawater. Geochim Cosmochim Ac 56, 2487-2501.

Voegelin, A.R., Nagler, T.F., Beukes, N.J., Lacassie, J.P., 2010. Molybdenum isotopes in late Archean carbonate rocks: Implications for early Earth oxygenation. Precambrian Res 182, 70-82.

Waldbauer, J.R., Sherman, L.S., Sumner, D.Y., Summons, R.E., 2009. Late Archean molecular fossils from the Transvaal Supergroup record the antiquity of microbial diversity and aerobiosis. Precambrian Res 169, 28-47.

Webb, G.E., Kamber, B.S., 2000. Rare earth elements in Holocene reefal microbialites: A new shallow seawater proxy. Geochim Cosmochim Ac 64, 1557-1565.

Wille, M., Kramers, J.D., Nagler, T.F., Beukes, N.J., Schröder, S., Meisel, T., Lacassie, J.P., Voegelin, A.R., 2007. Evidence for a gradual rise of oxygen between 2.6 and 2.5 Ga from Mo isotopes and Re-PGE signatures in shales. Geochim Cosmochim Ac 71, 2417-2435.

Wopenka, B., Pasteris, J.D., 1993. Structural Characterization of Kerogens to Granulite-Facies Graphite - Applicability of Raman Microprobe Spectroscopy. Am Mineral 78, 533-557.

Zerkle, A.L., House, C.H., Brantley, S.L., 2005. Biogeochemical signatures through time as inferred from whole microbial genomes. Am J Sci 305, 467-502.

Zhong, S.J., Mucci, A., 1989. Calcite and Aragonite Precipitation from Seawater Solutions of Various Salinites - Precipitation Rates and Overgrowth Compositions. Chem Geol 78, 283-299.

Ziegler, K., Chadwick, O.A., Brzezinski, M.A., Kelly, E.F., 2005. Natural variations of delta Si-30 ratios during progressive basalt weathering, Hawaiian Islands. Geochim Cosmochim Ac 69, 4597-4610.

ACKNOWLEDGMENT

This work was financed by DFG project SCHO 1071/4-1 and the Carl Zeiss Foundation. U. Horstmann provided carbon and oxygen isotope data of drill cores BH-1, GKP01 and GKP01. Comments by S. Schröder and an anonymous reviewer helped to significantly improve the quality of this publication. R. Parrish is thanked for editorial handling of the manuscript. F. Huettemann, M. Saeussele, S. Schafflick, D. Schoeckle and B. Steinhilber assisted with sample preparation and analyses. Scott Schlorholtz conducted XRD analyses at the Material Analyses and Research Lab (MARL) at the Iowa State University. This project benefited from helpful discussion with I. Kleinhanns and W. Wu.

FIGURE CAPTIONS

Figure 1: (a) Geological overview of Transvaal Supergroup lithologies and the Bushveld igneous complex in Southern Africa (modified from Eroglu et al. (2015)). (b) Cross section through chemical sediments of the lower TSG and schematic location of drill cores and the Kuruman Kop, modified after Beukes and Gutzmer (2008)

Figure 2: Raman data (I_D/I_G vs. FWHM-D) of marine sediments from the Malmani Subgroup (TA) and the Campbellrand Subgroup (GWA), as well as Raman spectra of characteristic lithologies. Changes in G- and D-bands imply a change in the disorder of carbonaceous matter and reveal higher peak metamorphic conditions for some samples (in particular mudrocks 665.3 and 673.0).

Figure 3: (a) Plot ($\delta^{18}O_{carb}$ vs. $\delta^{13}C_{carb}$) of KMF-5 and BH-1 carbonates analyzed for this study (after Fischer et al. (2009)). $\delta^{18}O_{carb}$ vs. $\delta^{13}C_{carb}$ data of GKP01 and GKP01 carbonates are from Fischer et al. (2009) and Horstmann and Beukes (2002). Data of all four drill cores greatly overlap and are interpreted and discussed in the text. Some distinctive trends show the influence of fluids on the $\delta^{18}O_{carb}$ signatures ("fluid alteration"), the influence of microbial induces organic carbon oxidation, likely dissimilatory iron reduction ("DIR" trend) on the $\delta^{13}C_{carb}$ trend. Some carbonate samples, in particular from the slope, plot between those two trends. Grey star indicates the average composition of Neoarchean seawater, based on estimates from Fischer et al. (2009), Shields and Veizer et al. (2002), and Veizer et al. (1999). (b) Illustration from Kasting et al. (2006) shows $\delta^{18}O$ signatures of marine calcites and calcitic fossils over the last 4 billion years. The thick line is the cubic smoothing spline evolution and authors suggest that values heavier than that represent pristine $\delta^{18}O$ signatures. The white diamond shows the $\delta^{18}O$ range of carbonates from CMCP with an average of about -8 ‰ relative to the VPDB standard.

Figure 4: Stratigraphic correlation and $\delta^{18}O_{carb}$ data of GKP01, GKF01, BH-1 (SACHA) and KMF-5. Triangles represent isotope data on carbonates of GKP01, GKF01 and BH-1 (SACHA) from Horstmann and Beukes (2002) and Fischer et al. (2009). Other isotope data of BH-1 and KMF-5 carbonates are from this study. Thin dashed black lines show stratigraphical correlations of formations, which belong to the Campbellrand-Malmani slope-platform succession. Thick dashed line indicates Kamden Member. VB: Vryburg; BP: Boomplaas; LM: Lokamonna; Monte.: Monteville; KN: Klein Naute; Ku: Kuruman; Kf.: Klipfonteinheuwel; Papk.: Papkuil; Kl: Klippan; Gh: Gamohaan; BR: Black Reef

Figure 5: Combined Raman (FWHM-D) and $\delta^{13}C_{org}$ data of carbonate (P-C: Pure carbonate, S-C: Silicified carbonate) and mudrock (MR) samples from KMF-5 (Malmani Subgroup, TA). Mudrocks provide overall lighter isotope values than carbonates except of two samples (665.3, 673.0), which also provide the lowest FWHM-D values. Solid boxes reflect $\delta^{13}C_{org}$ isotope range of GKP01, GKF01,

BH-1 and KMF-5 (black boxes: mudrocks, white boxes: carbonates). Isotope data of GKP01 and GKF01 are from Fischer et al. (2009). '?' completes the full range of measured $\delta^{13}C_{org}$ isotope values, however these heavier values might be rather a sign of ^{12}C-loss due to metamorphic overprint. Isotope ranges of most common microbial communities (ABP: Anoxygenic photoautotroph bacteria) indicate a mixed $\delta^{13}C_{org}$ signal and probably change in dominance of microbial organisms, with dependence on water depth and lithology (Freeman et al., 1990; Hayes, 2001; Robinson et al., 2003; Scott et al., 2004; Sirevag, 1995; Tabita, 1999; Valentine et al., 2004)

Figure 6: $\delta^{13}C_{carb}$, $\delta^{13}C_{org}$ and TOC data of carbonate and mudrock samples from GKP01 and GKF01 (slope) and BH-1 and KMF-5 (platform). Stratigraphy for GKP01, GKF01, and BH-1 is modified from Fischer et al. (2009). Black dashed lines mark the correlated sequences of all drill cores. Isotope data of GKP01, GKF01 and most of BH-1 are from Fischer et al. (2009) or are provided by Uwe Horstmann. The box included in the legend reflect the $\delta^{13}C$ isotope range of common marine microbial species, grey shaded area marks the range in which $\delta^{13}C_{org}$ data of CMCP samples fall (Thomazo et al. (2009) and references therein), relative to CO_2. APB: anoxygenic photoautotrophic bacteria, Pat: photoautotrophic bacteria (e.g. cyanobacteria), SRB: sulfur-reducing bacteria, MgB: Methanogenic bacteria, MtB: Methanotrophic bacteria. (Formations: VB-Vryburg; BP-Boomplaas; LM-Lokamonna; Monte-Monteville; KN-Klein Naute; Ku-Kuruman; Fairfi.-Fairfield; Kf.-Klipfonteinheuwel; Papk.-Papkuil; K.-Klippan; Gh-Gamohaan; BR-Black Reef).

Figure 7: Pure carbonate samples from this study plotted into a Sr/Ca vs. Mn diagram, after Veizer et al. (1989). "Limestone", "dolomite" and "siderite – Fe dolomite" fields are from Veizer et al. (1989). Here, we included "peritidal" and "shallow subtidal" fields. Note that samples falling into the "siderite" field are not siderites, as the Fe contents are too low (0.08 to 1.49 wt-% Fe), but rather dolomite with somewhat higher Fe contents.

Figure 8: Fe# ($[Fe_{tot}/(Fe_{tot}+Mn_{tot})]$) data of slope and platform sediments reveal a dependence on water depth and source water influx. Data of GKP01 and GKF01 are from Voegelin et al. (2010)

Figure 9: Simplified paleoenvironmental reconstruction of the CMCP over time with relative influxes of open ocean and freshwater. Thereby, REE+Y data of slope and platform sediments reveal a dependence on water depth and source water influx. The CMCP can be subdivided into the lower and the upper CMCP, deposited during four stages. During stage 1, the flooding of the Kaapvaal Craton, the high influx of hydrothermal water from the open ocean decreases with the build-up of the platform, visible on the REE+Y spectra of the Oaktree formation. In stage 2, the influence of continental material increases and is reflected in the REE+Y spectra of mudrocks and carbonates of the Monte Christo formation. At the same time, the carbonates from the subtidal Reivilo formation show signatures typical for shallow seawater, e.g. a positive Y anomaly, and carbonates from the slope reveal by a magnitude higher REE concentrations compared to the shelf carbonates, likely because they were more exposed to open ocean water. The deposition of the Kamden Member (Stage 3) during a short intense transgression marks the increased influx of open ocean water and hydrothermal fluids. During stage 4 of platform development, a rimmed margin formed, which limited the influx of open ocean water so that the influx of riverine water from the continent relatively increased. Data of GKP01 and GKF01 are from Voegelin et al. (2010).

Figure 10: $\delta^{13}C_{carb}$, $\delta^{13}C_{org}$ data of all slope and platform drill cores, divided into lower and upper CMCP. a) Box and whisker plots of $\delta^{13}C_{carb}$ values ; b) Mean values (with 2σ SD) of $\delta^{13}C_{carb}$, $\delta^{13}C_{org}$ from carbonates ($\delta^{13}C_{org-C}$) and from mudrocks ($\delta^{13}C_{org-MR}$) ; c) Box and whisker plots of $\delta^{13}C_{org}$ from carbonates (white boxes) and mudrocks (grey boxes) from the lower CMCP; d) Box and whisker plots of $\delta^{13}C_{org}$ from carbonates (white boxes) and mudrocks (grey boxes) from the upper CMCP. Three grey data points are from mudrocks of KMF-5 representing the upper CMCP. All data from GKP01 and GKF01, and most $\delta^{13}C_{carb}$ data of BH-1 are from Fischer et al. (2009) and Horstmann and Beukes (2002).

FIGURE CAPTIONS OF SUPPLEMENTARY MATERIAL

Figure S1: TOC content, oxygen and carbon isotope signature of carbonates and organic matter of KMF-5 samples. BR: Black Reef

Figure S2: TOC content, oxygen and carbon isotope signature of carbonates and organic matter of BH-1 samples. Abbreviations of Formations: BP: Boomplaas; LM: Lokamonna; Monte.: Monteville; Kf.: Klipfonteinheuwel; Papk.: Papkuil; Kl: Klippan; Gh: Gamohaan

Figure S3: XRD pattern of three representative carbonate samples from KMF-5 show a dolomite-quartz mixture with minor amounts of calcite. No Fe-minerals could be detected with this method.

Figure S4: Thin section images of representative carbonate samples from KMF-5, BH-1, and Kuruman Kop.

(1) Micritic laminated stromatolite with small cavities filled with silica, which are of lighter color than the surrounding matrix.

(2) Like (1), but heavily silicified. Migration of the silica appears unidirectional, following intercrystalline pores, presumably from stromatolitic carbonate layers and from cracks. Silicification occurred during early diagenesis, and reflects peritidal conditions.

(3) Laminated fine-grained carbonate, with small silica-filled cavities and stylolites that originate from pressure dissolution after carbonate formation.

(4) Laminated fine-grained carbonate with small peloid-like carbonate debris trapped and bound by microbial laminae. Stylolites originate from pressure dissolution after carbonate formation.

(5) Laminated fine-grained agglutinated stromatolite. Small peloids are of microbial origin and are typical for trapping and binding of particles (mostly carbonate debris) in the microbial mats. This represents wave-agitated facies between shallow subtidal to intertidal conditions.

(6) Fine microbial laminations, partly showing silicification, which is indicative for peritidal conditions.

(7) Fine micritic carbonate with organic-and detritus-rich layer, following lamination.

(8) Alternating dark and light laminated carbonate layers, finely crystallized with coarsely crystalline fenestral structures. Such structures typically represent intertidal to lagoonal facies.

(9) Fenestrae-rich carbonate in fine-grained micritic matrix. Some fenestrae are lined by thin, dark microbial laminae. Depositional conditions were intertidal to lagoonal.

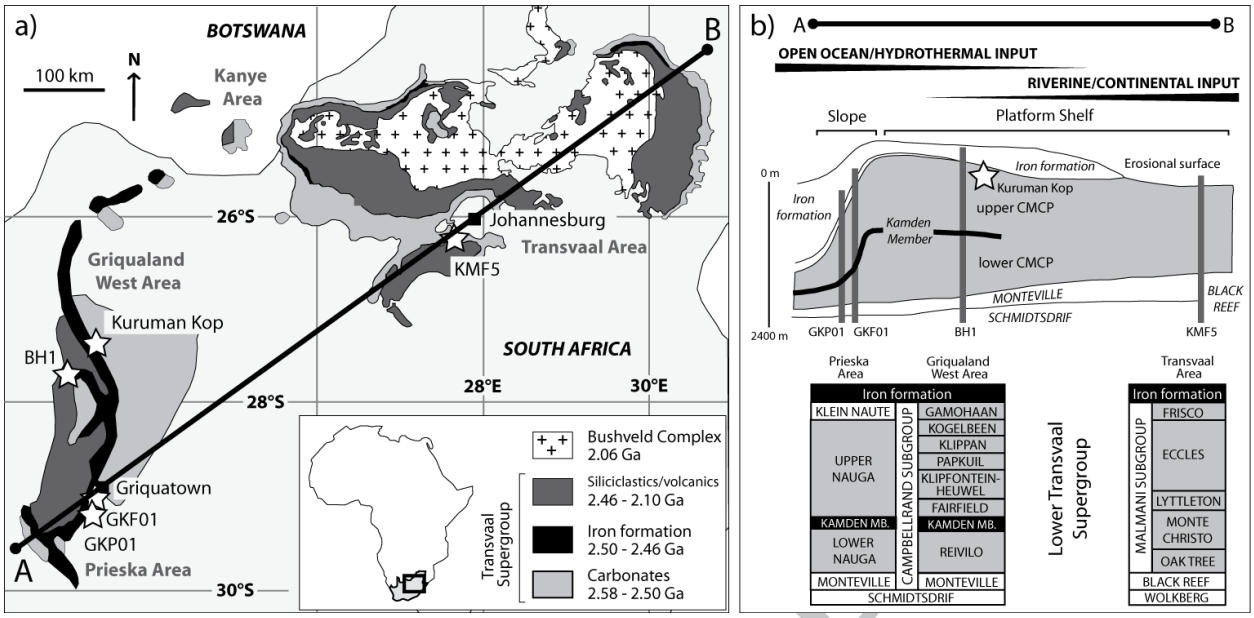

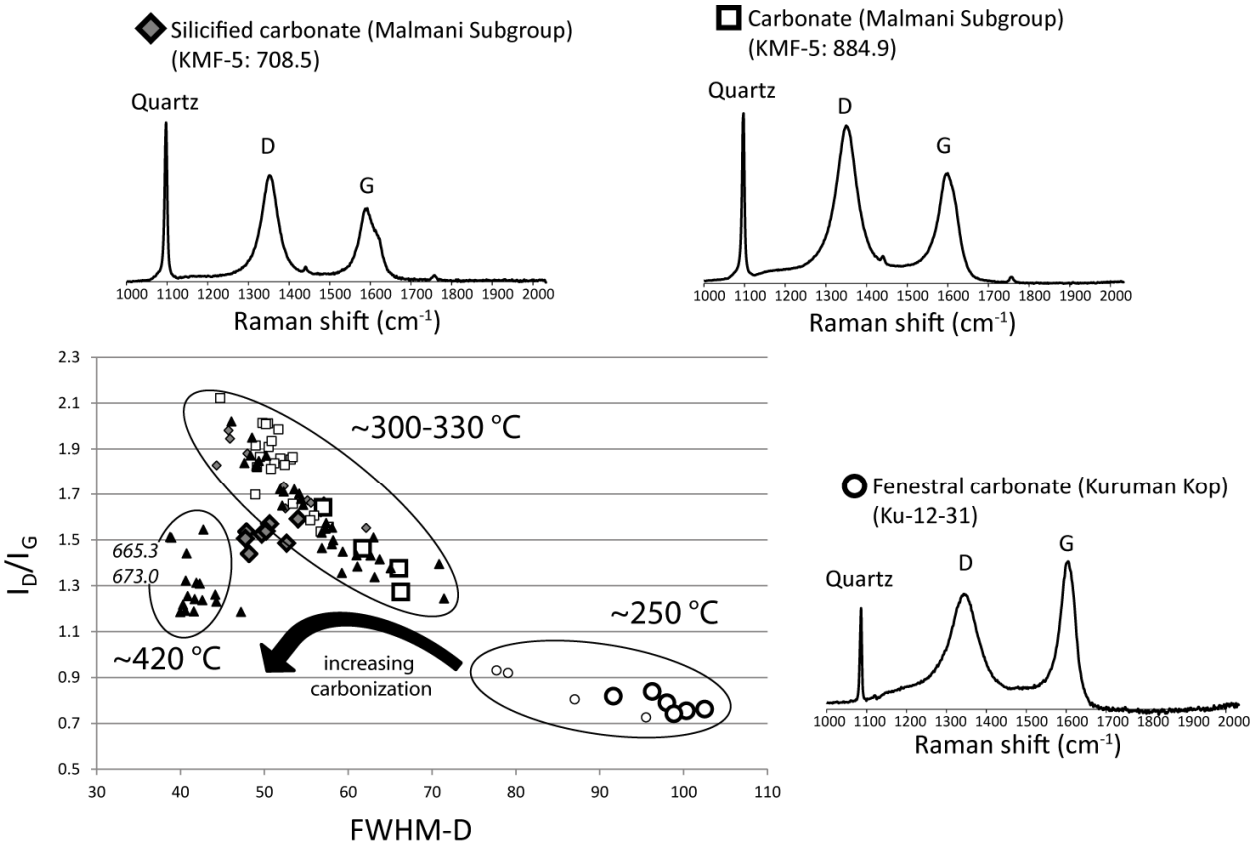

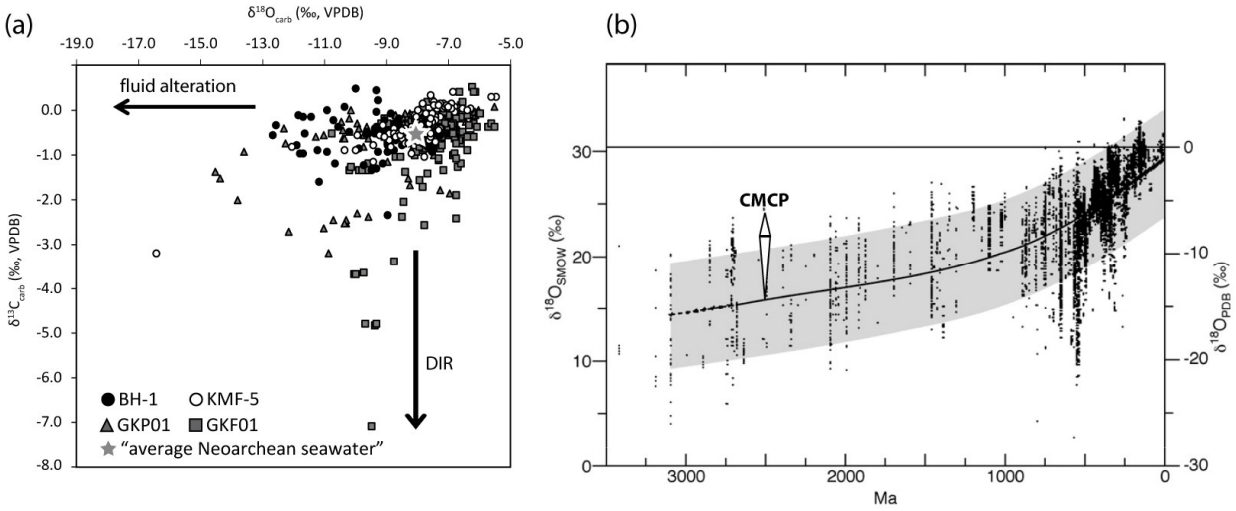

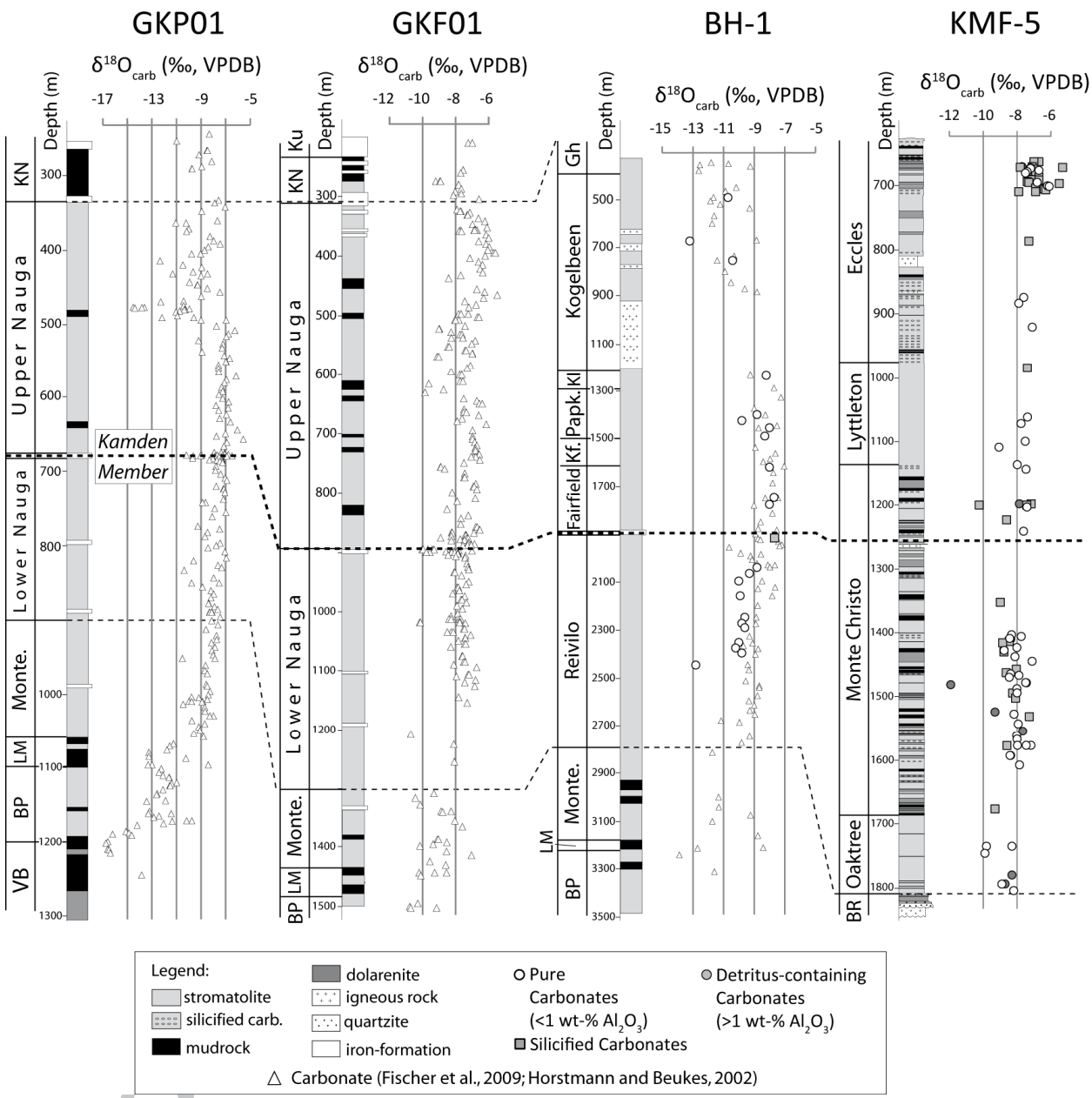

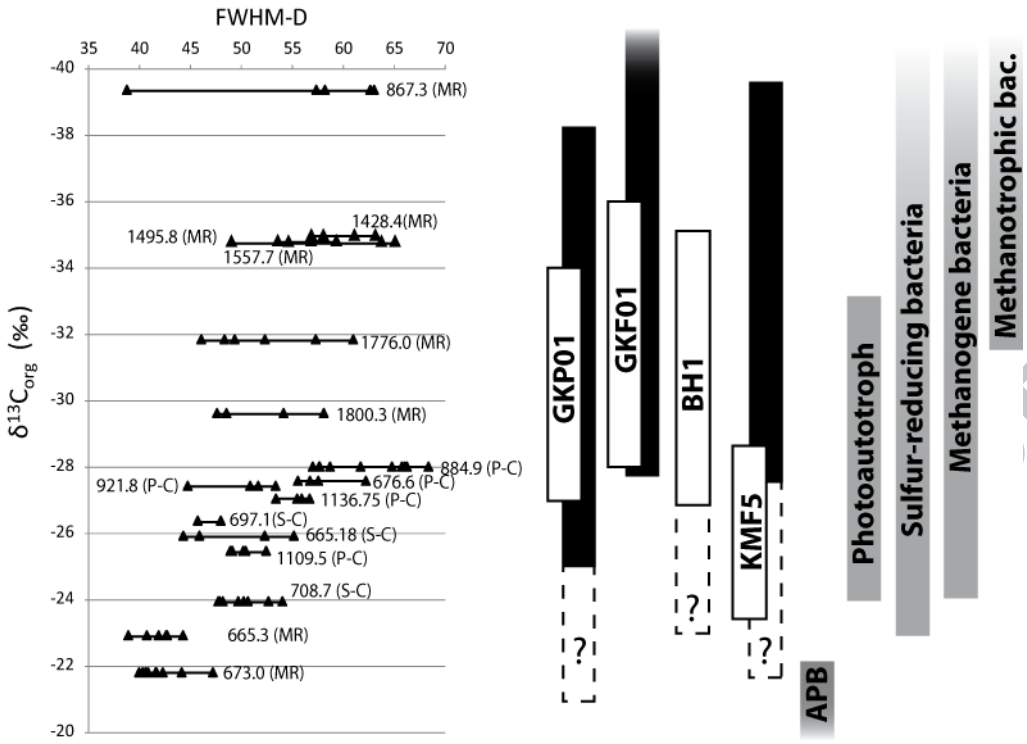

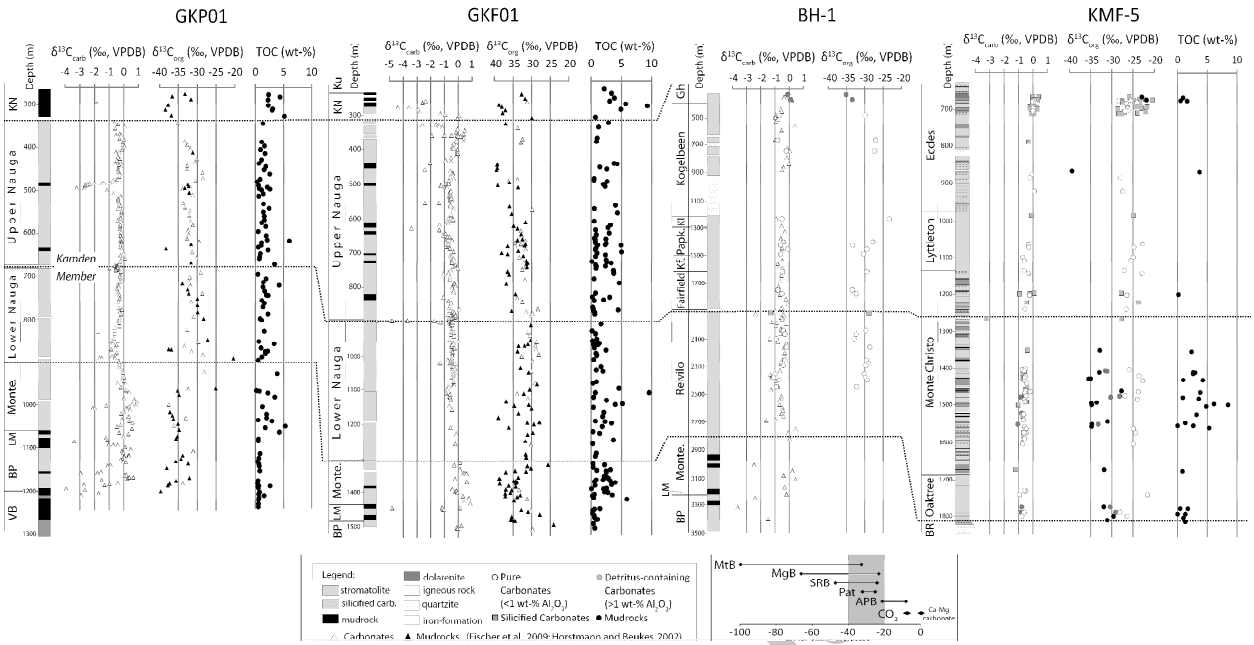

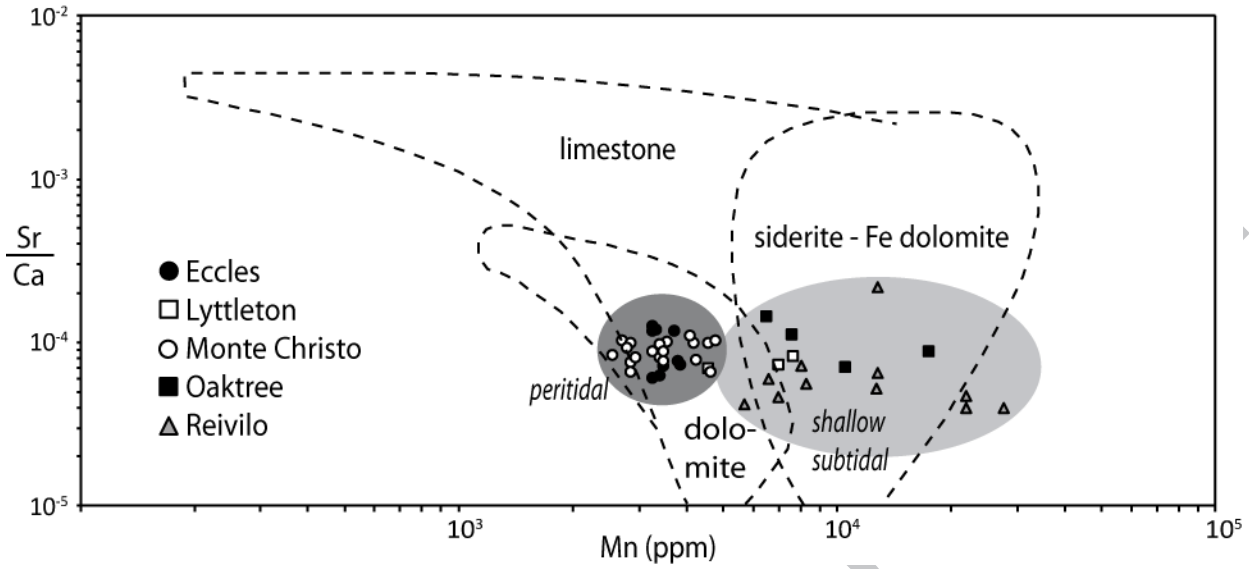

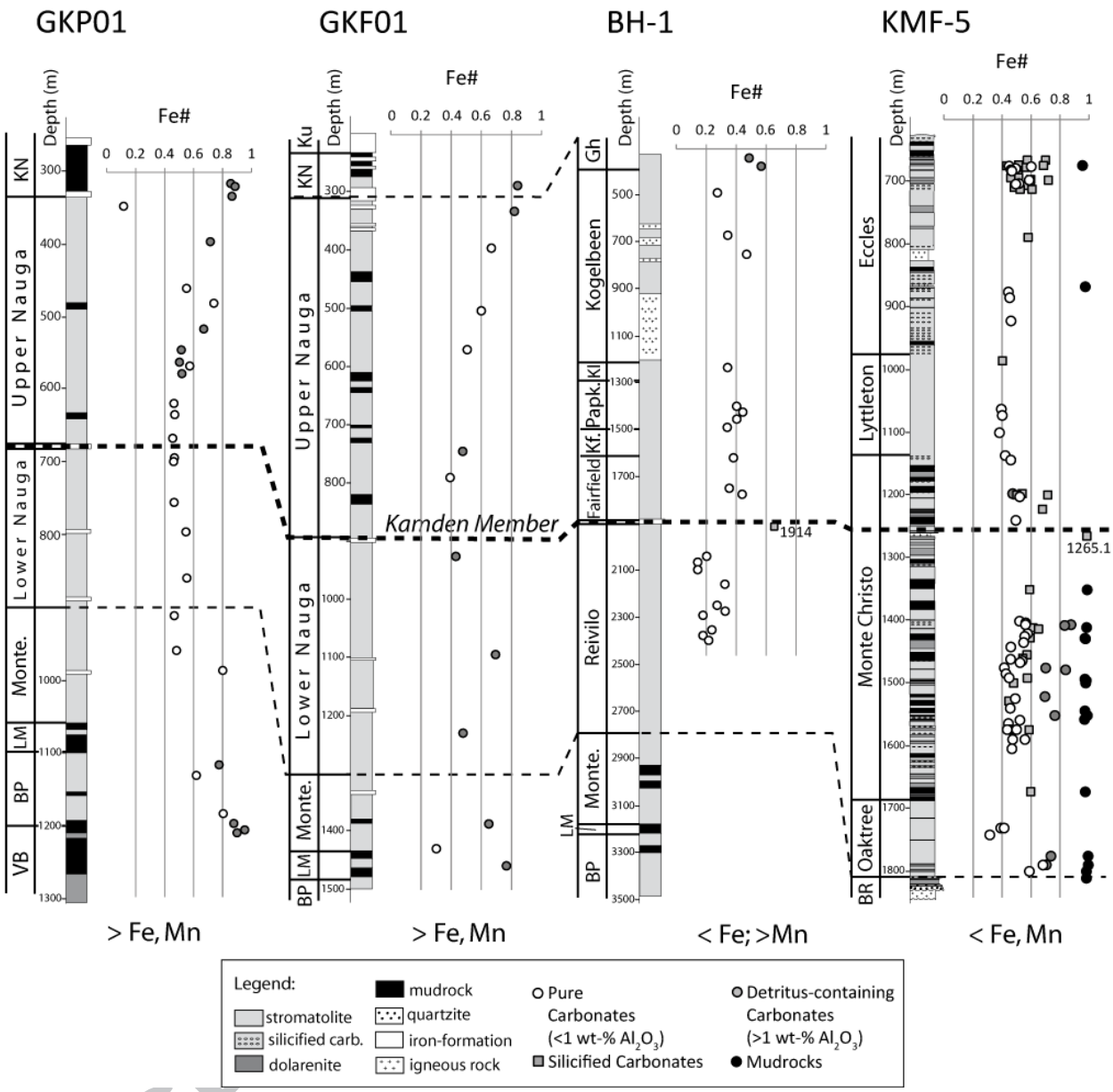

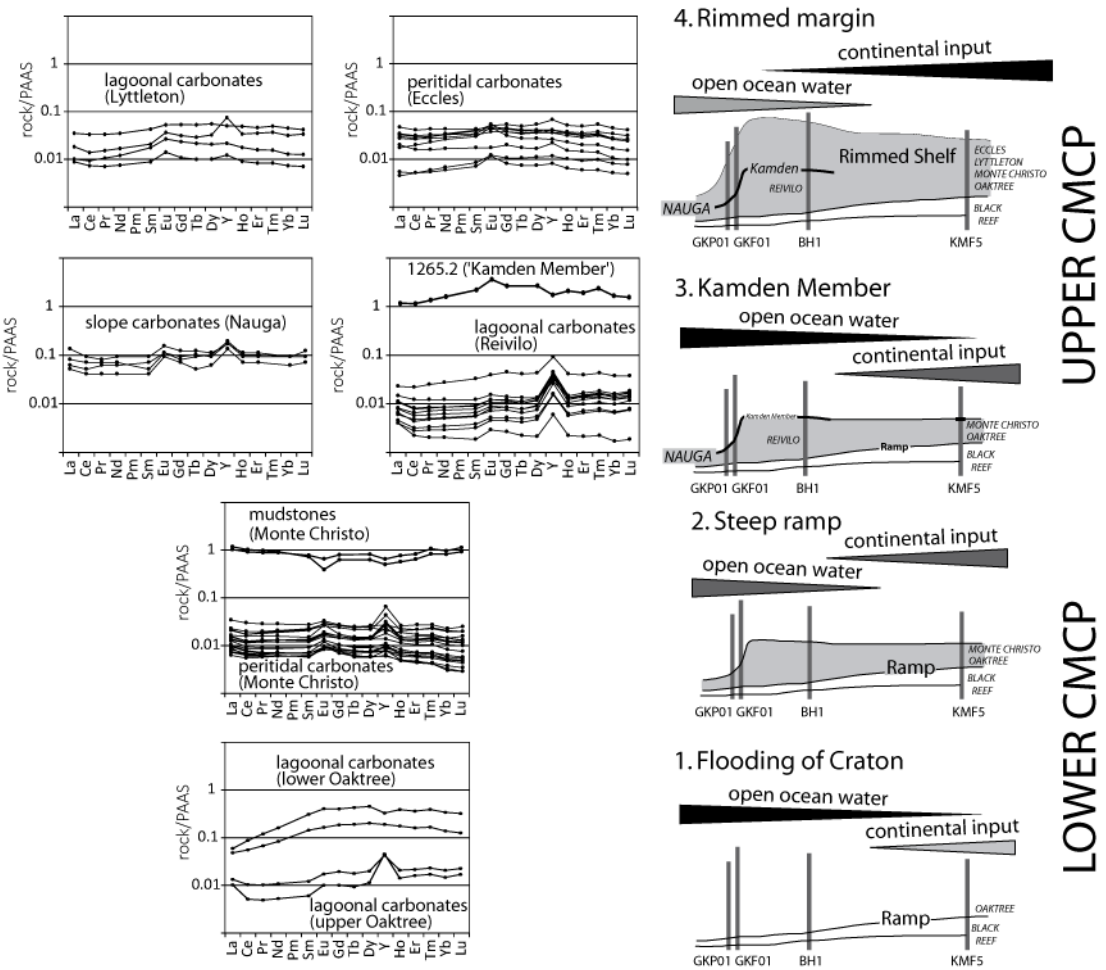

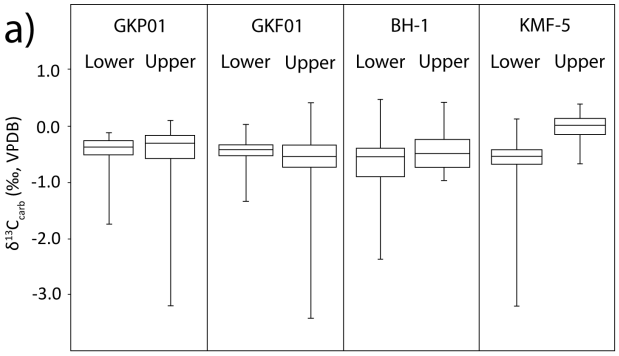

b)

	BH-1			KMF-5		
	$\delta^{13}C_{carb}$	$\delta^{13}C_{org\text{-}C}$	$\delta^{13}C_{org\text{-}MR}$	$\delta^{13}C_{carb}$	$\delta^{13}C_{org\text{-}C}$	$\delta^{13}C_{org\text{-}MR}$
Upper	-0.47 ± 0.64 ‰ (N=56)	-30.15 ± 6.63 ‰ (N=13)	N/A	-0.03 ± 0.47 ‰ (N=38)	-25.31 ± 4.30 ‰ (N=35)	-28.03 ‰ (N=3)
Lower	-0.69 ± 0.90 ‰ (N=53)	-30.16 ± 2.92 ‰ (N=12)		-0.63 ± 0.85 ‰ (N=55)	-29.70 ± 5.67 ‰ (N=8)	-32.81 ± 4.53 ‰ (N=15)

	GKP01			GKF01		
	$\delta^{13}C_{carb}$	$\delta^{13}C_{org\text{-}C}$	$\delta^{13}C_{org\text{-}MR}$	$\delta^{13}C_{carb}$	$\delta^{13}C_{org\text{-}C}$	$\delta^{13}C_{org\text{-}MR}$
Upper	-0.60 ± 1.57 ‰ (N=83)	-30.73 ± 3.11 ‰ (N=27)	-32.61 ± 4.14 ‰ (N=10)	-0.60 ± 1.09 ‰ (N=144)	-32.16 ± 3.71 ‰ (N=26)	-35.31 ± 6.17 ‰ (N=34)
Lower	-0.46 ± 0.61 ‰ (N=71)	-30.99 ± 3.29 ‰ (N=12)	-30.78 ± 9.53 ‰ (N=11)	-0.49 ± 0.50 ‰ (N=74)	-30.19 ± 3.30 ‰ (N=13)	-31.93 ± 5.14 ‰ (N=26)

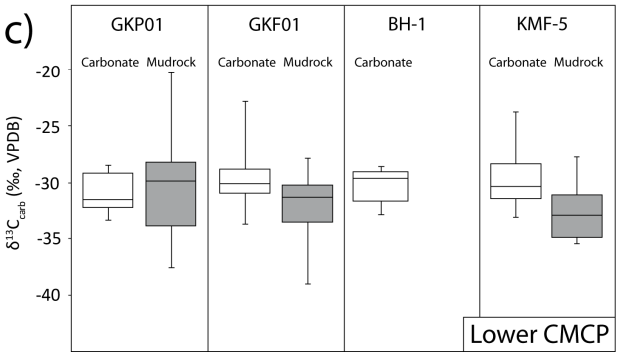

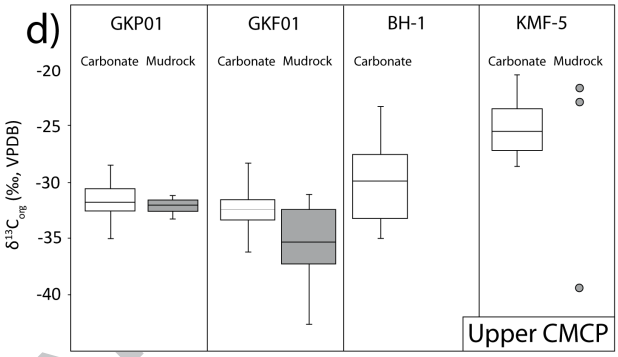

Highlights

- Carbon cycle of Neoarchean carbonate platform and potential oxygen oasis
- Carbon isotopes reveal a shift to aerobic biosphere and increasing oxidation state
- Rare earth element patterns reveal decrease in open ocean water influx
- Rimmed margin architecture was crucial for evolution of aerobic ecosystems